Seismic Response Meta-Model of High-Rise Fame Structure Based on Time-delay Neural Network

He Zhang[a], Marius Bittner[b], Michael Beer[c]

[a] Ph.D., Lecturer, College of Civil Science and Engineering, Yangzhou University, 225127 China (E-mail: scottz14@126.com, scottz14@163.com)

[b] Ph.D student, Institute for Risk and Reliability, Leibniz University Hannover, Hannover 30167, Germany (E-mail: bittner@irz.uni-hannover.de)

[c] Professor, Institute for Risk and Reliability, Leibniz University Hannover, Hannover 30167, Germany; Institute for Risk and Uncertainty, Adjunct Professor, University of Liverpool, Peach Street, L69 7ZF Liverpool, United Kingdom; Adjunct Professor, International Joint Research Center for Engineering Reliability and Stochastic Mechanics, Tongji University, Shanghai 200092, China

[*]Correspondence should be addressed to He Zhang; scottz14@126.com

Abstract

To make structural seismic response simulation more efficient, a meta-model model method which is based on the time delay neural network is proposed. And an accuracy evaluation method that considers the drift peak amplitudes and maximum amplitudes in each intensity as performance parameters is also proposed, this method can make a balance between accuracy and training time. Exampled by 4 frame structures which are all 20 stories, and accuracy evaluating results show that more than 80% of samples, which include training models and testing models of these performance parameters can be explained by meta models' fitting. The average time to simulate by this method is 0.08s and faster than the finite element method which spends 24 min averagely.

Keywords: Metamodel, neural network, seismic, frame structure, SRC-RC frame

1. Introduction

Earthquakes are one of the most dangerous natural hazards for building structures. The seismic damage to frame structures, which are the most widely used structural forms, is a relationship between interstory deformation and bearing capacity. Performance-based seismic design is a formal process for the design of new buildings, or seismic upgrades of existing buildings, which includes a specific intent to achieve defined performance objectives in future earthquakes (FEMA P.58 2012). Performance objectives should be based on resisting seismic technical methods and economic conditions and should relate to building uses, seismic precautionary intensity, the degree of structural irregularity and structural types, ductility requirements, manufacturing cost, and reparability after expected earthquakes (GB50011 2010). The process includes defining performance objectives, conceptual design, objective checking calculation and analysis, and structural seismic reliability analysis. With the improvement of computers and the requirements of structural design, reliability analysis, such as Monte Carlo analysis, has been introduced to structural engineering. Furthermore, in the last 30 years, China has built a huge monitoring system for earthquakes, and the transmission time of earthquake data can obviously be reduced by 5G communications technology, which provides early warning structural safety by simulating the structural response in the transmission time difference between the 5G signal and the earthquake vibration. These two areas require as fast a calculation speed as possible. However, the traditional methods to simulate structural seismic responses are based on methods such as finite element methods (FEMs), such as beam elements with plastic hinges (Powell, G. H. 1986), and finite fiber elements (Rahman, M.M. 2021) are not efficient enough.

The relationship between earthquake signals such as ground motion acceleration time histories and structural responses such as frame structure interstory drift can be treated as a time series functional

relationship. When a structure is in elastic status, the relationship is a group of linear differential equations, and beginning in elastoplastic status, the functional relationship changes to be complex. The neural network is a method to imitate the input-output relationship of a system (White, H 2014). In addition, the neural network is efficient (Pomerleau, D. 1991), and advances are developable (Kikkawa, H. 1993). The structural response calculation process can be treated as inputting earthquake signals to the structural system and outputting response data.

To predict structural seismic responses, meta models based on recurrent neural networks (RNNs) and a long short-term memory network (LSTM), which is a special kind of RNN (Sherstinsky, A, 2020), have been proposed, such as Zhang R. (2019) predicted responses of a steel moment resisting frame by LSTM and Huang Y. (2021) predicted shake table test results of slope (Zhou J. 2019) by RNN. For small and simple systems, their prediction results are well matched. However, Molina D. (2011) made a comparison of the time-delay neural network (TDNN) and RNN to predict dynamic responses of power systems. RNN was not observed to offer noticeable improvements in the precision of the identified model for systems with dynamics and coupling relationships, and TDNNs can converge faster by a suitable training method when applied to large systems. The relationship between ground motions and responses of a high-raise frame structure can be treated as a kind of coupling system, and the future structural response that will happen is related not only to the future signals but also to the loading and response histories that have happened. Thus, this process is suitable to be imitated by time-delay neural networks (TDNNs) (Chen y. 2010), which can evaluate the effect of histories on new outputs.

However, for large and compound systems such as the seismic response of high-rise frame structures, it is difficult to realize that each time step is the same, in addition to setting up a large-scale neural network that has multiple hidden layers and contains a large number of neurons. However, its

training time is also large. Thus, a method to balance the training time and accuracy must be proposed. It is important to evaluate whether the results are acceptable, and an accuracy evaluation method must be proposed.

The most widely used objective to divide the structural performance (damage) level is interstory drift, which was adopted by the Chinese “Code for seismic design of buildings” (GB50011 2010) and “PRESTANDARD AND COMMENTARY FOR THE SEISMIC REHABILITATION OF BUILDINGS” (FEMA356 2000). Based on interstory drift, the failure boundaries of SRC-RC hybrid frame structures, which are a type of frame structure in which lower story columns are made of steel reinforced concrete (SRC) and upper story columns are made of reinforcd concrete (RC), have been proposed by Zhang, H. (2019-a). These failure boundaries correspond to three seismic resistance requirements (failure levels) of GB50011:

(1) Level 1, for the requirement “no damage after structure suffers frequent earthquakes”, failure boundaries are structural elastic bearing capacity and its elastic drift limit value 1/550;

(2) Level 2, for the requirement “repairable after structure suffer moderate earthquakes”, failure boundaries are structural elastoplastic drift limit value 3/550; and

(3) Level 3, for the requirement “no collapse after structure suffers rare earthquakes”, failure boundaries are structural collapse drift limit value 2.0%.

Thus, an accuracy evaluation method that can evaluate whether the results of the TDNN-based metamodel are acceptable can be proposed based on interstory maximum drift values with a serious earthquake input.

In this paper, taking Zhang, H. (2019-a) SRC-RC frame structure schemes that are 20 stories, 5×5 spans as an example, a method to build metamodels for relationships between earthquake acceleration

signals and interstory drift in high-rise frame structures by using time-delay neural works is introduced, and a method to evaluate the fitting accuracy of the models has been proposed.

2. Method to establish and train TDNN Metamodel

2.1 Architectures of TDNN

Time delay neural network (TDNN) (Waibel, A. 1989) is a multilayer artificial neural network architecture whose purpose is to classify patterns with shift invariance and model context at each layer of the network. In the time series problem that is addressed by the TDNN, the predicted values of $y(t)$ from the previous values of $x(t)$ are shown in Eq.1. In addition, d is the delay number.

$$y(t) = f(x(t-1)..., x(t-d)) \quad \textbf{(1)}$$

Fig. 1 is the architectures of TDNN. R is the number of elements in the input vector, S is the number of neurons in the layer, **P** is the input vector, **IW** is the input weight matrix, **LW** is the layer weight matrix, **a** is the output vector, **b** is the bias vector, and TDL is the tapped delay lines (Mayhan, J. 1981). **a** is labeled **y**. Layers in the TDNN play different roles. The layer that produces the network output (the last layer) is called the output layer, and all other layers are called hidden layers. The layer that links and transfers input data is called the input layer; normally, it is the first layer in the network (Shoaib, M. 2019). In each layer i, the jth neuron has a summary that gathers its weighted inputs and bias to form its scalar output $\mathbf{n}(i,j)$. The various $\mathbf{n}(i,j)$ taken together form an S-element net input vector $\mathbf{n}(i)$. f_i is the logical function of layer i.

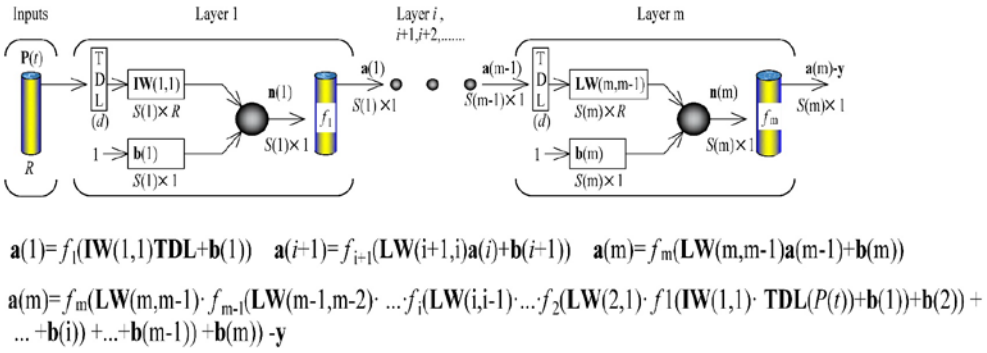

$$\mathbf{a}(1)=f_1(\mathbf{IW}(1,1)\mathbf{TDL}+\mathbf{b}(1)) \quad \mathbf{a}(i+1)=f_{i+1}(\mathbf{LW}(i+1,i)\mathbf{a}(i)+\mathbf{b}(i+1)) \quad \mathbf{a}(m)=f_m(\mathbf{LW}(m,m-1)\mathbf{a}(m-1)+\mathbf{b}(m))$$

$$\mathbf{a}(m)=f_m(\mathbf{LW}(m,m-1)\cdot f_{m-1}(\mathbf{LW}(m-1,m-2)\cdot \ldots \cdot f_i(\mathbf{LW}(i,i-1)\cdot \ldots \cdot f_2(\mathbf{LW}(2,1)\cdot f1(\mathbf{IW}(1,1)\cdot \mathbf{TDL}(P(t))+\mathbf{b}(1))+\mathbf{b}(2)) + \ldots +\mathbf{b}(i)) +\ldots+\mathbf{b}(m-1)) +\mathbf{b}(m)) -\mathbf{y}$$

Fig. 1 Architectures of TDNN

2.2 Process of frame seismic response simulation by TDNN instead of FEM

There are two methods to prepare TDNN models for a multiple story frame structure, as shown in Fig. 2: set one neural network for entire structures and set individual networks for stories. The first method can respond to all compound relationships between stories, but the neural network is large and can simulate complex and nonlinear systems, and its training time is much longer than training of individual networks.

As shown in Fig. 2, earthquake accelerations are treated as input data for TDNN model training, and interstory drifts of each story are selected and treated as target data for each TDNN model training. Each story can output two directions (x and y) of data, for all are 2*n* groups. Thus, for each story, two networks were set up corresponding to the x- and y-directions. In addition, these 2*n* networks construct a TDNN group NETS. When new earthquake acceleration signals are put into the TDNN group NETS, each interstory drift response of the structure will be outputted, as shown in Fig. 3.

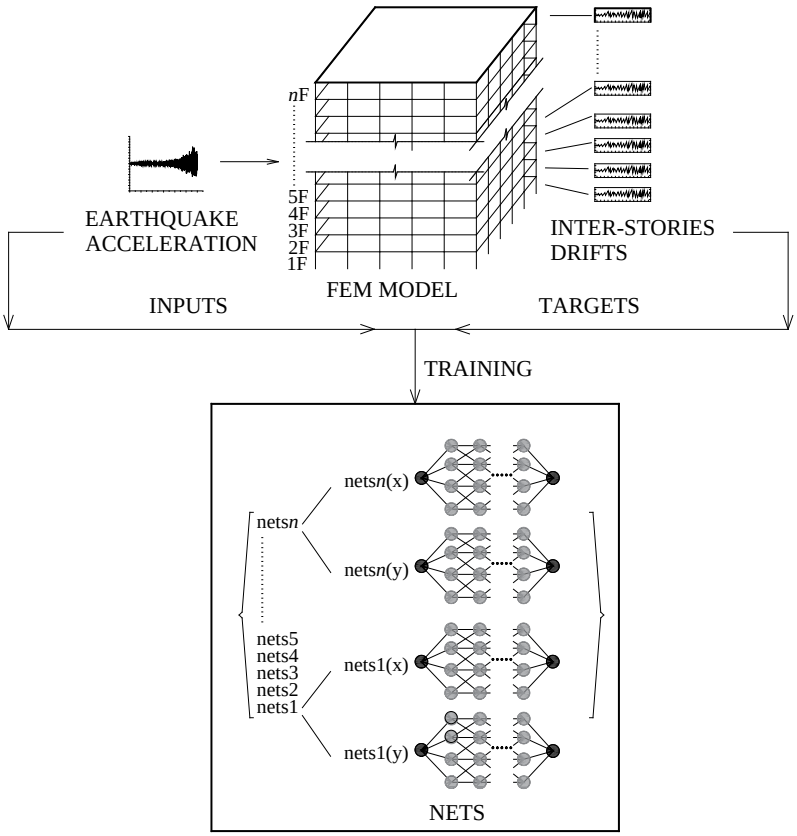

Fig. 2 Database of TDNN Metamodel

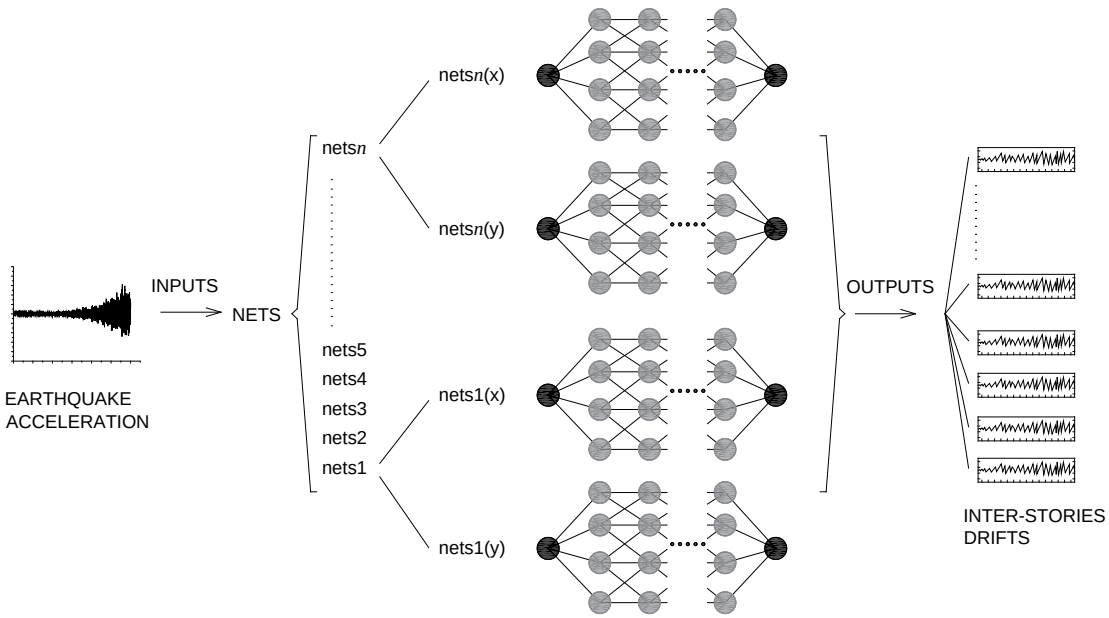

Fig. 3 Structural seismic response simulation by the TDNN Metamodel

2.3 Training method of TDNN Metamodel

The software MATLAB provides two methods to train the TDNN: batch training and incremental training (Wei, Z. 2017). Batch training, in which weights and biases are updated only after all the inputs and targets are presented, cannot be adjusted in the training process. If new data are collected and used for training the trained network, new data should be combined with old data and input to a new training process. However, in incremental training, the weights and biases of the network are updated each time an input is presented to the network, which provides access to add and renew data each time (MathWorks 2021).

As it is shown in Fig.4, for time-delay networks, the time vector is an unshown independent variable in addition to input data. Thus, the sorting of input data will influence network training results. When databases are set up for each earthquake event, its structural responses are calculated individually, which means inputting one earthquake event EQ_1, and the FEM output response RS_1, and then the FEM model will initialize to be non-damage status. It is the same for EQ_2, …., EQ_m, and their structural responses RS_2, …., RS_m, respectively. Each EQ_i-RS_i couple is not time-correlated to others. However, if the TDNN group NETS is trained by the batch method, earthquake events will be put into one matrix side by side such as $IP = \{ EQ_1, EQ_2, \ldots, EQ_m, \}$, and the same method will be applied to their structural responses to obtain the target database, such as $TG = \{RS_1, RS_2, \ldots, RS_m\}$. But it makes a time order for earthquake events when the TDNN reads them that from EQ_1 to EQ_2 and to… EQ_{m-1} is the earliest to later and the last. For batch training to *IP* and *TG* and *d* is the number of TDNN time delays, d time-step columns of data at the last DB_1 are considered, which is the database corresponding to EQ_1 as the initial state of DB_2, which is the database corresponding to EQ_2. However, its initial value is no earthquake acceleration, and no structural deformation before EQ_2 occurred. This error will also appear at the beginning of any other

database DB_i. Furthermore, to an n-story structure, its input is a $1\times\sum_{i=1}^{m} st_i$ matrix, its target is a $1\times\sum_{i=1}^{m} st_i\times n$ matrix and st_i is the number of time steps of DB_i. The entire database is huge and requires a long time spent for training, and the collection of data is complex and expensive (Guo, H. 2019). Thus, the batch training method is not suitable for this type of model.

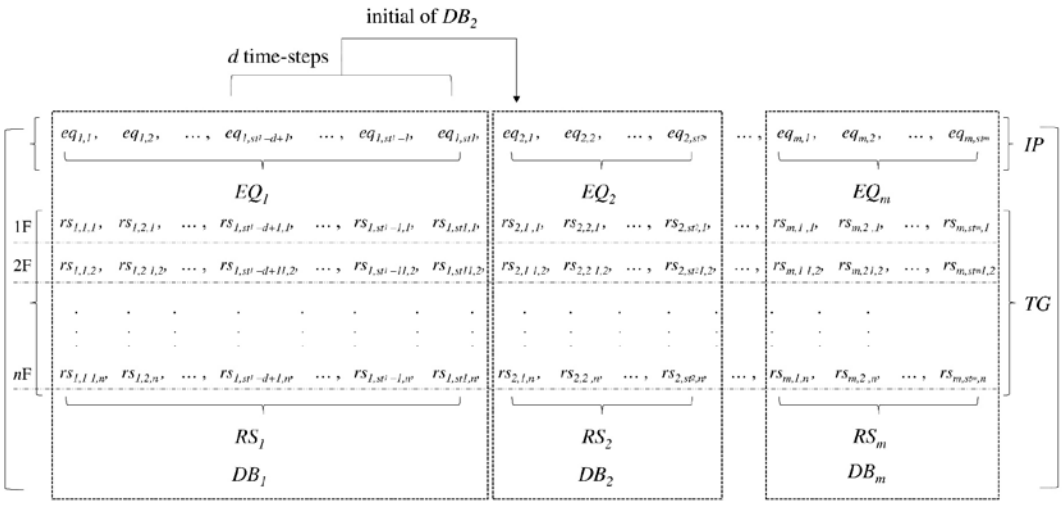

Fig. 4 Time order for earthquake events when TDNN reading databases by batch training

Fig. 5 shows the training process for incremental training. In the beginning, $\text{NETS}_{(0)}$ is the initial TDNN group, the first database DB_1 is inputted, then $\text{NETS}_{(0)}$ is adapted to be $\text{NETS}_{(1)}$ according to DB_1, DB_2, DB_3,…, DB_m by turns, and IW. Ir is the input weight parameter of NETS in this training, which defines the learning parameters and values for the current learning function of the input layer's weight coming from the input and DB_1, r_1 is the Pearson product-moment correlation coefficient of $\text{NETS}_{(1)}$ output, and training target RS_1. Then, DB_2 is inputted, $\text{NETS}_{(1)}$ is adapted to $\text{NETS}_{(2)}$, and the Pearson product-moment correlation coefficient r_2 of this adaptation process is calculated. DB_3,…, DB_m are sequentially inputted, $\text{NETS}_{(2)}$,…, $\text{NETS}_{(m-1)}$ are sequentially adapted, r_2,…, r_m is calculated, and finally, $\text{NETS}_{(m)}$ is obtained. Then, $\text{NETS}_{(m)}$ is treated as the new initiative to be $\text{NETS}_{(0)}$ and begins a new cyclic

adaptation. When the minimum value of r_1, r_2, r_3,…, r_m is larger than the required value [r], the adapting cycle will break, the training is finished, and the final trained TDNN group NETS is obtained. If new earthquake signals are inputted into the NETS, a structurally predicted response can be outputted. When the new database DB_{m+1} is selected, NETS can be treated as the new initiative to be $NETS_{(0)}$, and new incremental training will begin with a new value of IW.Ir. By incremental training, networks can be renewed for lifelong learning (Chen, Z. 2016) and will be "Learning without Forgetting" (Li, Z. 2017).

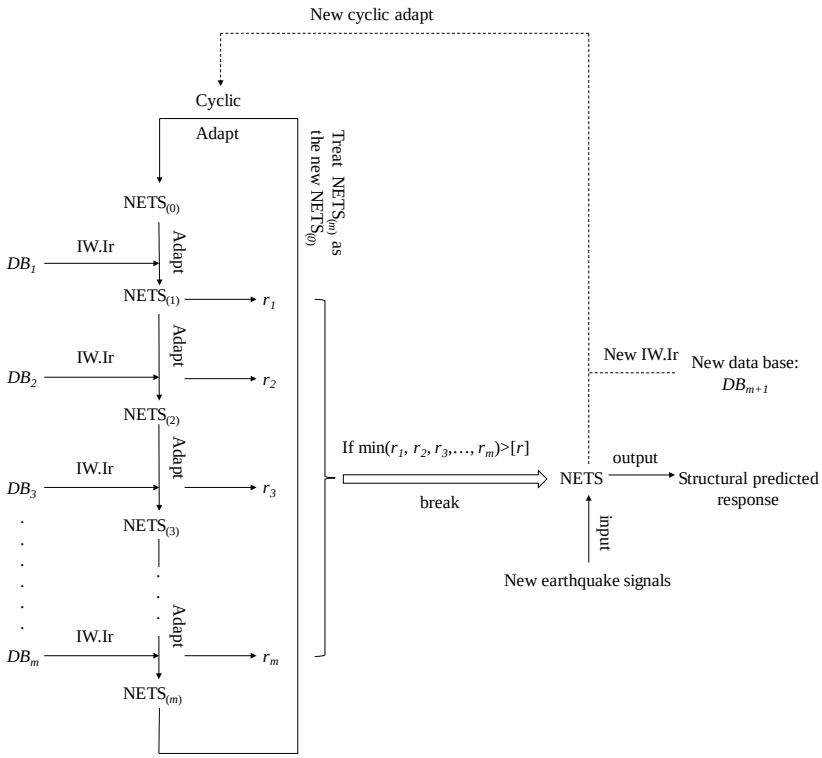

Fig. 5 The training process of incremental training

3. Accuracy evaluation method with examples

3.1 Data-based FEM models

Four design schemes (M_0, M_1, M_2, and M_3) of a 5×5 span and 20 story frame structure are treated as case studies, and their layout is shown in Fig. 6. For all schemes, beams are reinforced concrete (RC). All columns in scheme M_0 are made of steel-reinforced concrete (SRC). Schemes M_1, M_2, and M_3 are three SRC-RC hybrid frames, which means columns in their lower stories are SRC made, and in their

upper stories are RC made, and between SRC stories and RC stories, there are SRC-RC transfer stories that are stiffness and bearing capacity transfer. In these transfer stories, there are SRC columns and SRC-RC columns that are made of SRC lower parts and RC upper parts. According to the research of Zhang, H. (2019-a), SRC-RC hybrid frame is good seismic performance and better construction costs. For M_1, M_2, and M_3, their SRC-RC transfer stories are between 10F~12F, as shown in Fig. 7. All these schemes match the design requirements of GB50011 and FEMA 356. The section of columns and beams is shown in Fig. 8. Models of these schemes were built in FEM (finite element method) analysis software SEISMOSTRUCT, and Table 1 shows the material properties. where E_c, E_s, and E_r are the elastic moduli of the concrete, steel, and reinforcement, respectively; f_{ck} is the axial compressive strength of the concrete, f_c is its designed value; f_{ys} is the yield strength of the steel, f_s is its designed value; f_{yr} is the yield strength of the reinforcement, and f_r is its designed value.

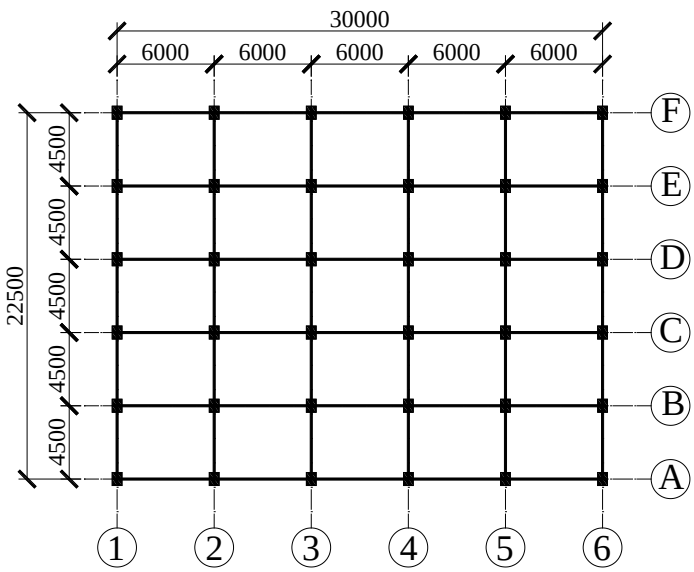

Fig. 6 Structural layout put of case studies

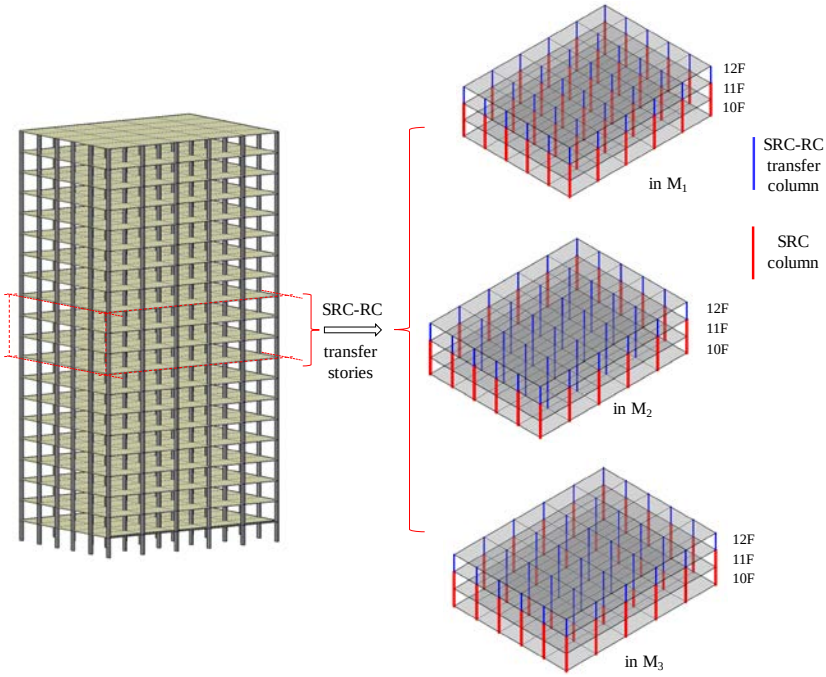

Fig. 7 SRC-RC transfer stories in M_1, M_2, and M_3

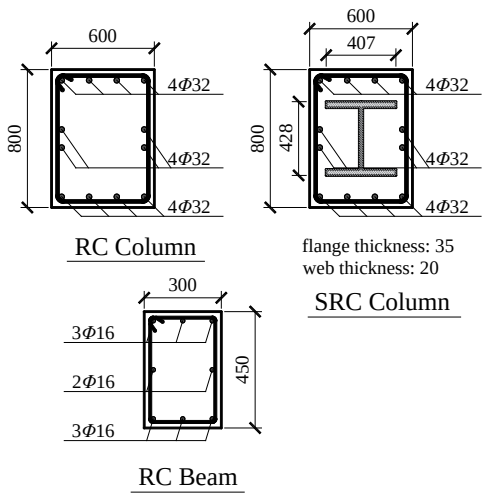

Fig. 8 Columns and beams sections of case studies

Table 1 Material Properties

Concrete			H-shaped Steel			Reinforcement Bars		
E_c	f_{ck}	f_c	E_s	f_{ys}	f_s	E_r	f_{yr}	f_r
$N\cdot mm^{-2}$	$N\cdot mm^{-2}$	$N\cdot mm^{-2}$	$N\cdot mm^{-2}$	$N\cdot mm^{-2}$	$N\cdot mm^{-2}$	$N\cdot mm^{-2}$	$N\cdot mm^{-2}$	$N\cdot mm^{-2}$
30×10^3	20.1	14.3	200×10^3	235	205	200×10^3	335	300

All frame members cross-section behaviors were represented by the fiber element, where each fiber was associated with a uniaxial stress-strain relationship; the sectional stress-strain state of the beam-column elements was then obtained through the integration of the nonlinear uniaxial stress-strain response of the individual fibers (typically 100−150), in which the section was subdivided (Zhang, H. 2019-b). Material constitutive models are the same as Zhang, H. (2019-a), that concrete follows the Mander et al. (1988) nonlinear concrete model (con_ma), and steel and reinforcements follow Menegotto and Pinto's (1973) steel model (stl_mp). In addition to training and testing earthquakes, a slab distribution load of 8.5 kN/m^2 is applied to represent the gravity of the concrete slab and decorative materials and live load.

3.2 Database preparation for Metamodel training

For the drift-based design method in standards of China (GB50011), Europe (EN1998-1), and America (FEMA 356), the maximum value of interstory drift is most interesting to designers and researchers. Most seismic damage indices are also related to the maximum deformation value once an earthquake occurs (Park, Y. 1985). In addition, according to the design method of Zhang, H. (2019-a), failure boundaries were built by drift limits. Thus, the target data and output data of TDNN groups are structural drifts between stories. To prepare training data, 4 earthquake acceleration signals $\{EQ_1\}$, $\{EQ_2\}$, $\{EQ_3\}$ and $\{EQ_4\}$ were generated. Each earthquake is generated by the random method of (Zhang, H. 2021) and has 120 s duration, its intensity (I) is gradient-increased from 4.5 degrees to 10 degrees, and the increment is 0.5 degrees per 10 s, as shown in Fig. 9. For each design scheme, M_0, $\{EQ_1\}$, $\{EQ_2\}$, $\{EQ_3\}$ and $\{EQ_4\}$ are individually inputted into its FEM model on Seismostruct, and their structural responses (interstory drifts) of M_0 $\{RS_{01}\}$, $\{RS_{02}\}$, $\{RS_{03}\}$ and $\{RS_{04}\}$ are calculated. With the same method as M_1, M_2 and M_3, responses [$\{RS_{11}\}$, $\{RS_{12}\}$, $\{RS_{13}\}$ and $\{RS_{14}\}$], [$\{RS_{21}\}$, $\{RS_{22}\}$, $\{RS_{23}\}$ and

{RS_{24}}] and [{RS_{31}}, {RS_{32}}, {RS_{33}} and {RS_{34}}] are calculated. The first three earthquake signals {EQ_1}, {EQ_2}, {EQ_3}, and their responses are treated as training databases, and the last earthquake signal {EQ_4} and its responses {RS_{04}, RS_{14}, RS_{24}, RS_{34}} are treated as testing databases to test the accuracy of Metamodels. Fig. 10 shows the structural responses calculated by the FEM models, which are treated as targets and testing data, and θ is the inter-story drift.

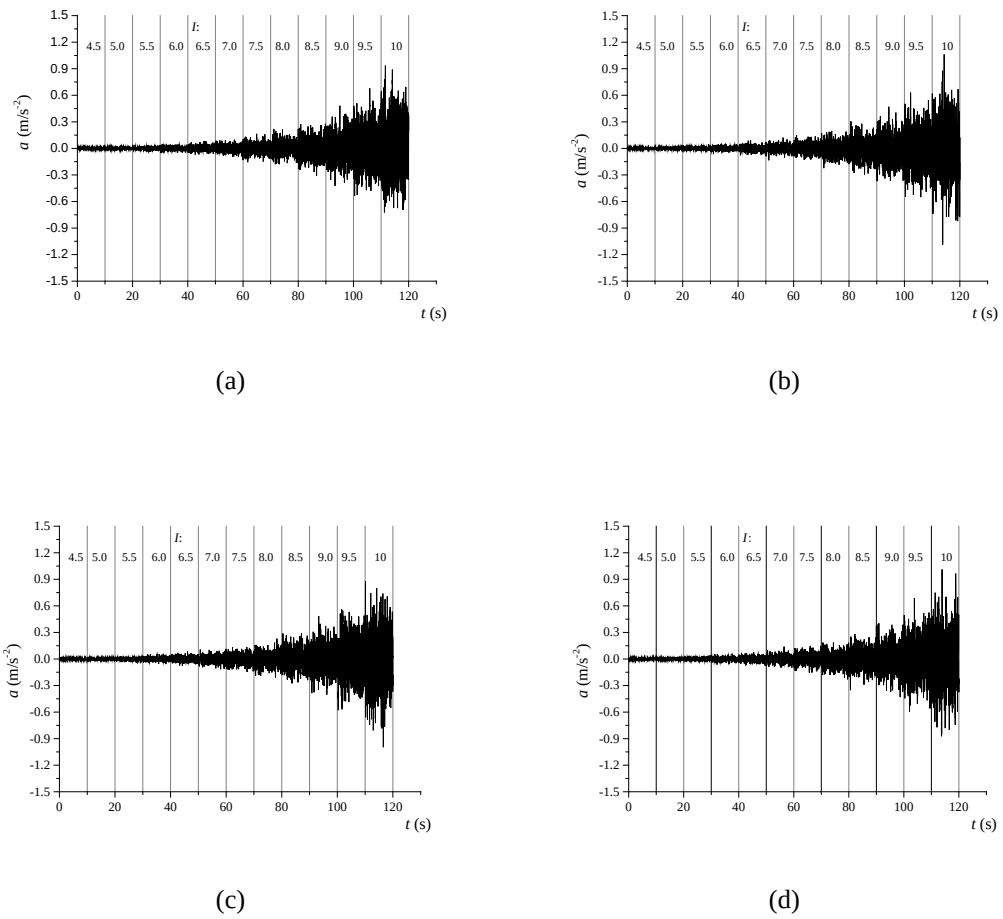

Fig. 9 Earthquake time history inputs: (a) {EQ_1}, (b) {EQ_2}, (c){EQ_3} and (d) {EQ_4}

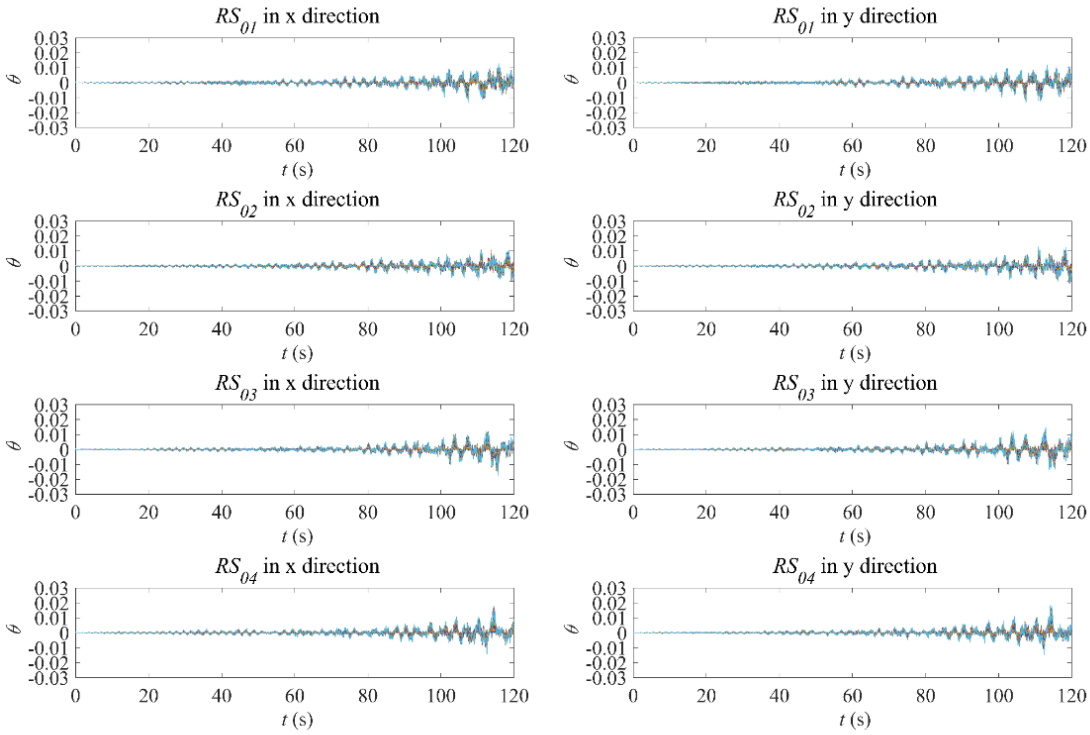
RS01 in x direction
RS01 in y direction
RS02 in x direction
RS02 in y direction
RS03 in x direction
RS03 in y direction
RS04 in x direction
RS04 in y direction
θ
t (s)

(a)

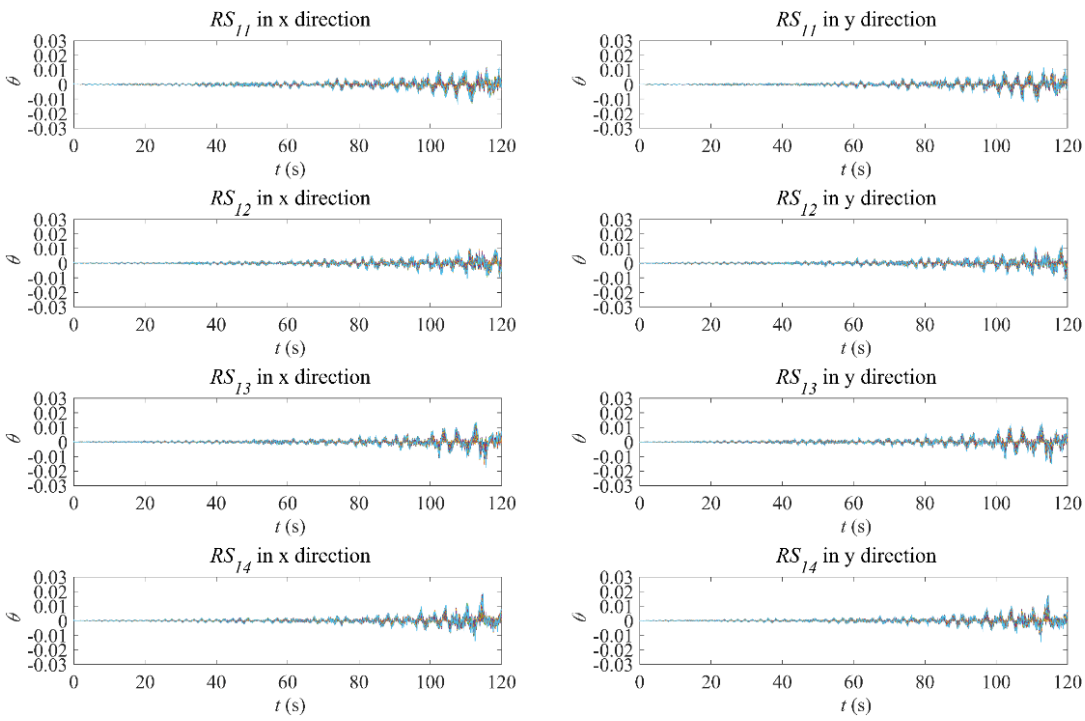
RS11 in x direction
RS11 in y direction
RS12 in x direction
RS12 in y direction
RS13 in x direction
RS13 in y direction
RS14 in x direction
RS14 in y direction
θ
t (s)

(b)

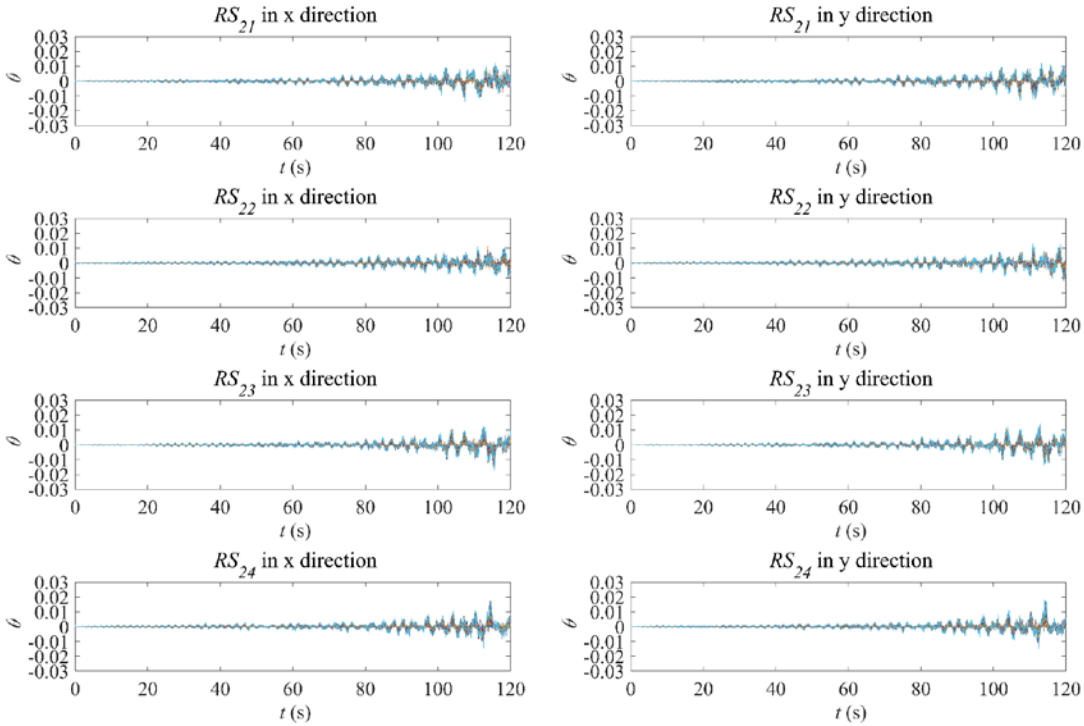

(c)

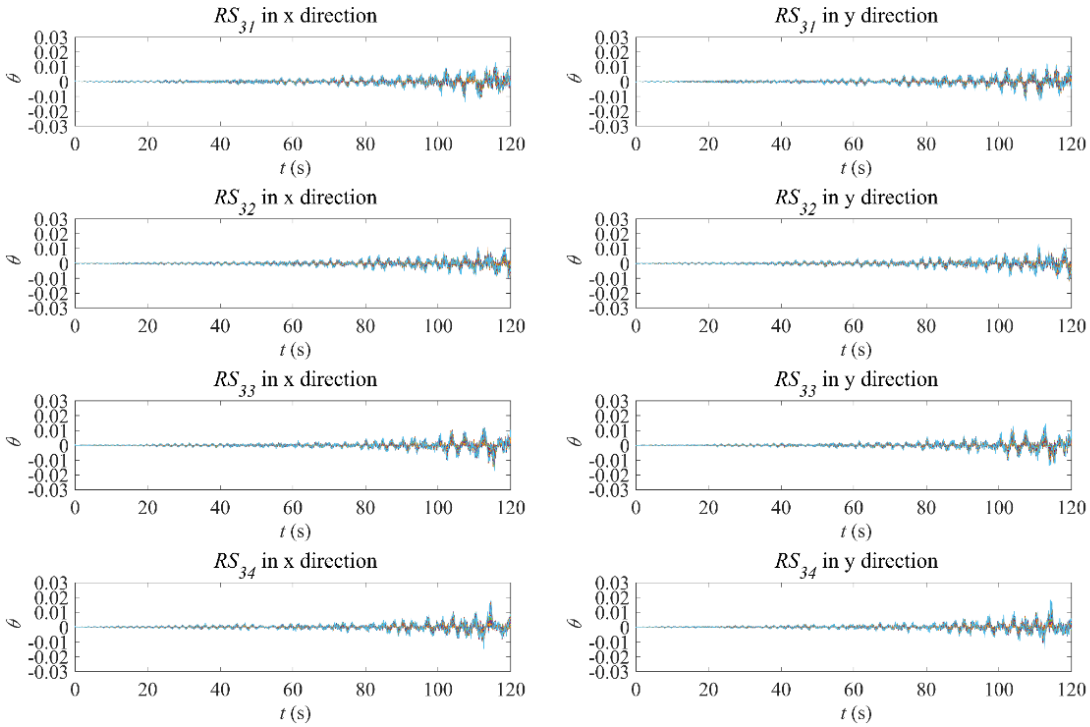

(d)

Fig. 10 Structural responses calculated by FEM models: (a) M_0; (b) M_1; (c) M_2; (e) M_3

3.3 Design of TDNN groups and outputs

There are TDNN groups for 4 schemes to be designed. Each building scheme M_i is 20 stories; thus, its response contains 20 stories of x-direction drifts and y-directions, and there are 40 networks in each TDNN group $NETS_{Mi}$. As shown in Fig. 11, for each TDNN group $NETS_{Mi}$, in each network nets*i*(x0) or nets*i*(y), in addition to the input layer and the output layer, there are 5 hidden layers, and each contains 4 neurons. In the training process, for each adaptation, IW. Ir is set as 0.7. Data bases $DB_{i1}=\{EQ_1, RS_{i1}\}$, $DB_{i2}=\{EQ_2, RS_{i2}\}$ and $DB_{i3}=\{EQ_3, RS_{i3}\}$ that correspond to $\{EQ_1\}$, $\{EQ_2\}$, $\{EQ_3\}$ are treated as training data, and their outputs from $NETS_{Mi}$ are $\{OUT_{i1}\}$, $\{OUT_{i2}\}$ and $\{OUT_{i3}\}$. Regression evaluations of $\{OUT_{i1}\}$, $\{OUT_{i2}\}$ and $\{OUT_{i3}\}$ to $\{RS_{i1}\}$, $\{RS_{i2}\}$ and $\{RS_{i3}\}$ are used to describe the fitting similarity. $\{EQ_4\}$ and its outputs from $NETS_{Mi}$ $\{OUT_{i4}\}$ are used to test the simulation accuracy of $NETS_{Mi}$. Fig. 12 is outputs by TDNN groups.

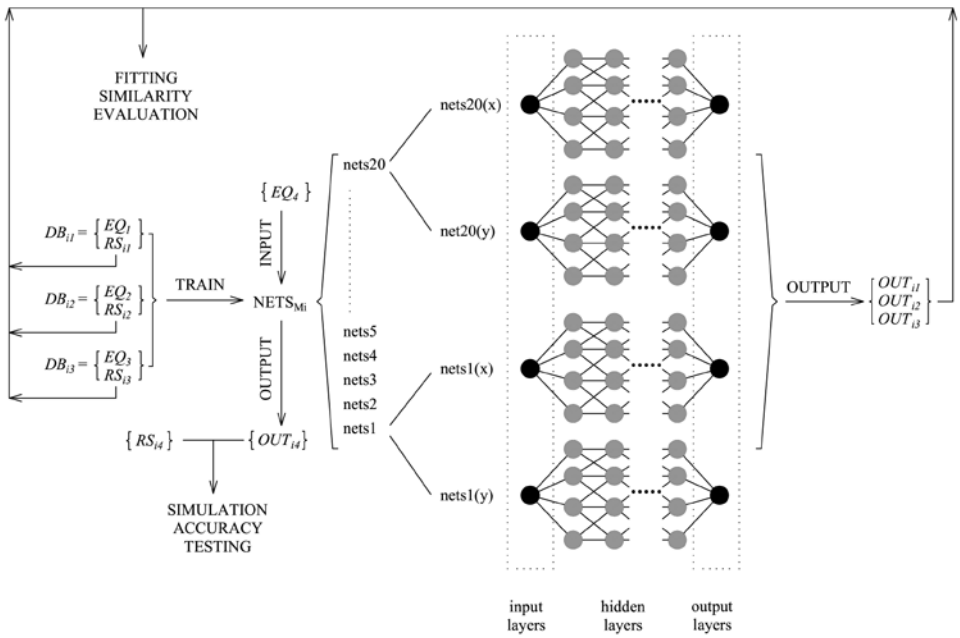

Fig. 11 Construction and training process of $NETS_{Mi}$

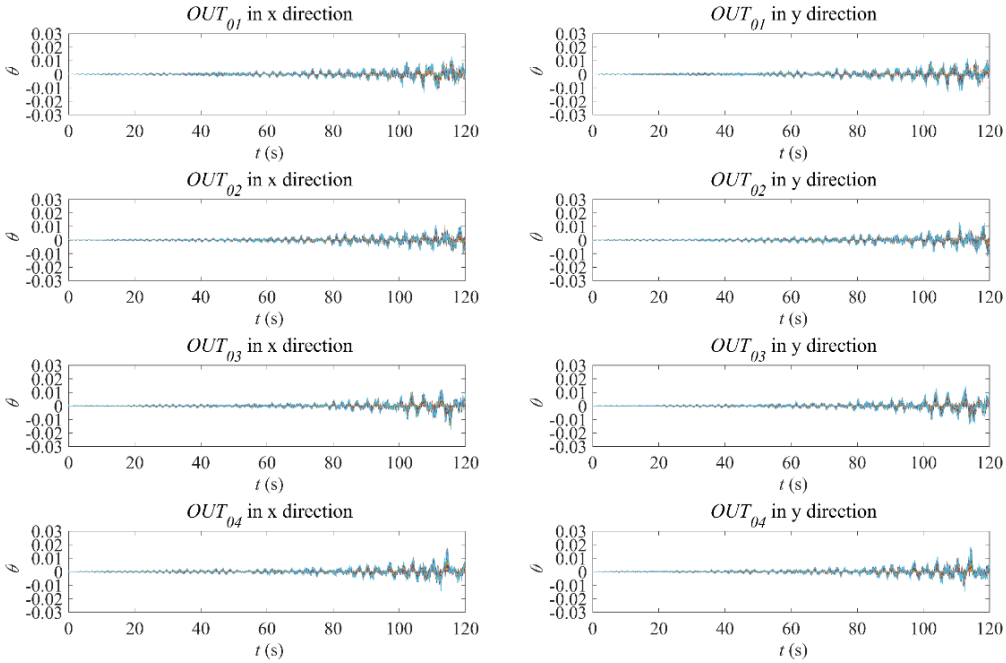
OUT01 in x direction
OUT01 in y direction
OUT02 in x direction
OUT02 in y direction
OUT03 in x direction
OUT03 in y direction
OUT04 in x direction
OUT04 in y direction
θ
t (s)

(a)

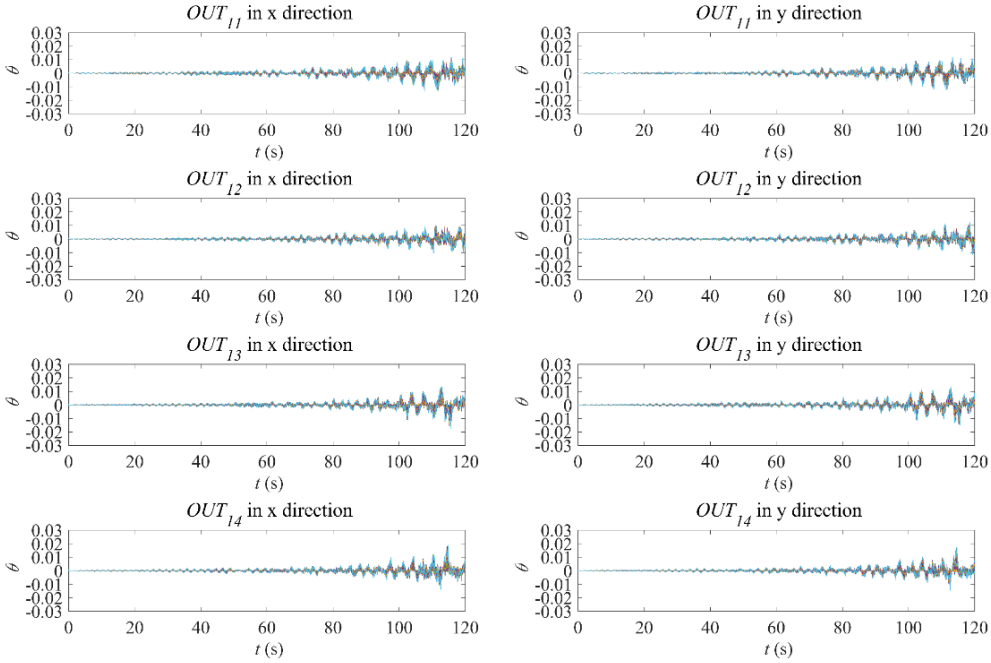
OUT11 in x direction
OUT11 in y direction
OUT12 in x direction
OUT12 in y direction
OUT13 in x direction
OUT13 in y direction
OUT14 in x direction
OUT14 in y direction
θ
t (s)

(b)

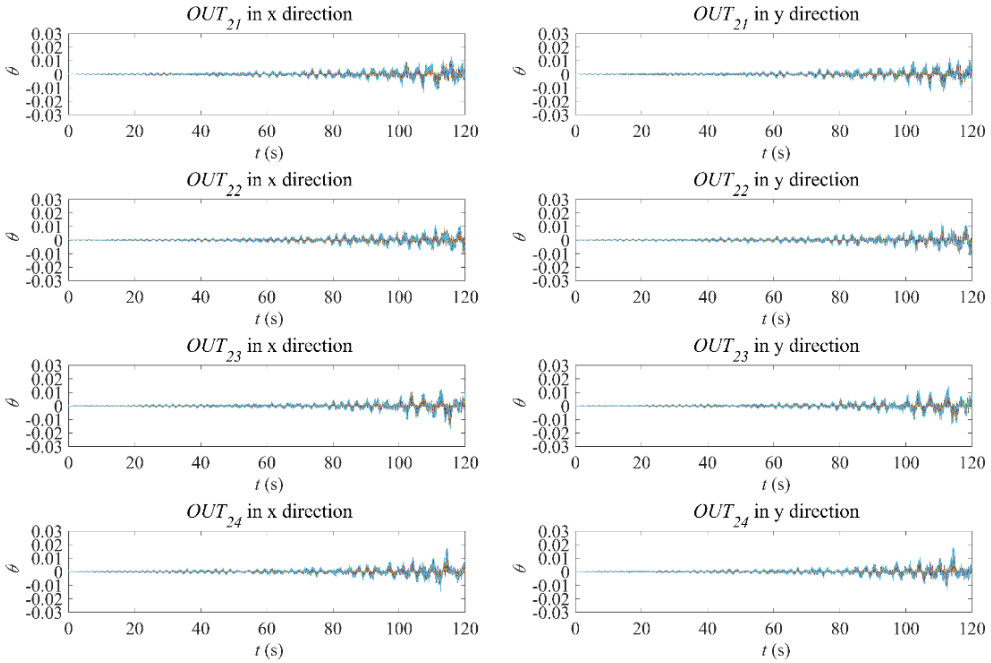

(c)

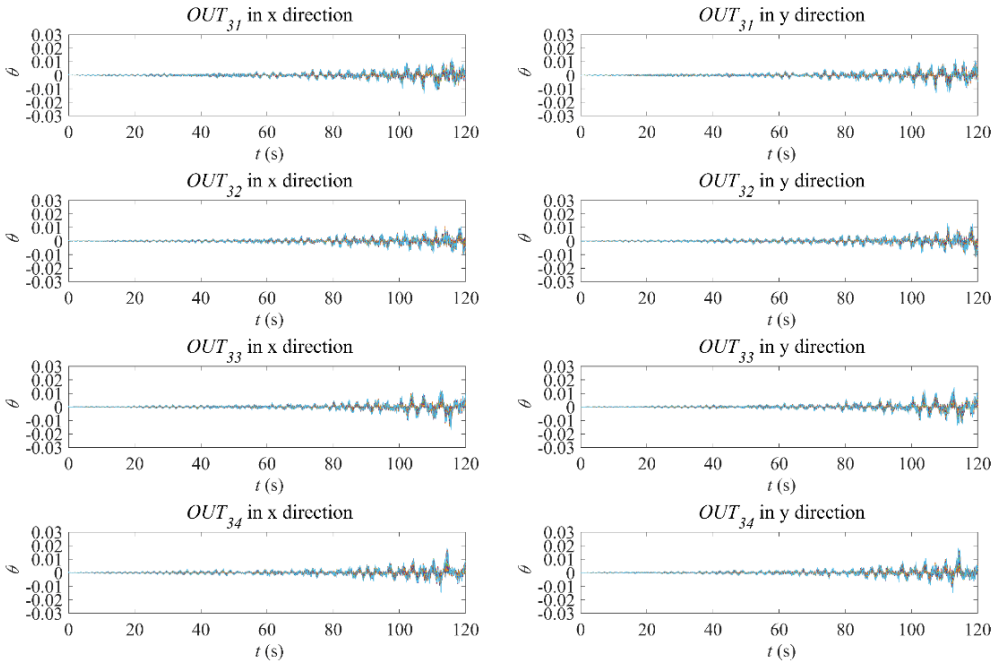

(d)

Fig. 12 Structural responses calculated by FEM models: (a) M_0; (b) M_1; (c) M_2; (e) M_3

3.4 Results and accuracy evaluation

To evaluate the simulation accuracy and fitting similarity of TDNN groups, performance measures must be selected. Each earthquake input{EQ_1}, {EQ_2}, {EQ_3} and {EQ_4} can be divided into 12 stages, in which the intensity varies from 4.5 to 10. Each FEM result and TDNN output can also be divided into 12 stages. According to GB50011 and FEMA 356, structural performance level evaluation conditions are based on maximum interstory drifts (θ_{max}). Table 2 shows θ_{max} values for failure boundaries corresponding to three levels in the Chinese standard GB50011. Thus, it is of interest to evaluate the simulation accuracy and fitting similarity of metamodels that are constructed by TDNN groups. Inside each stage, earthquake amplitude changes are not drastic. Amplitude θ_{peak} is the absolute value of the extrema of interstory drift inside of a stage, as shown in Fig. 13, and it does not change drastically, either. Thus, θ_{peak} is also treated as a performance measure to evaluate the simulation accuracy and fitting similarity of metamodels that are constructed by TDNN groups. Based on the safety evaluation method of GB50011 and FEMA 356, the TDNN models fit the FEM models well if their θ_{max} and θ_{peak} of each stage are well matched.

Table 2 θ_{max} values for failure boundaries stipulated by GB50011

Failure levels	θ_{max} values (%)
Level 1	0.18
Level 2	0.54
Level 3	2.00

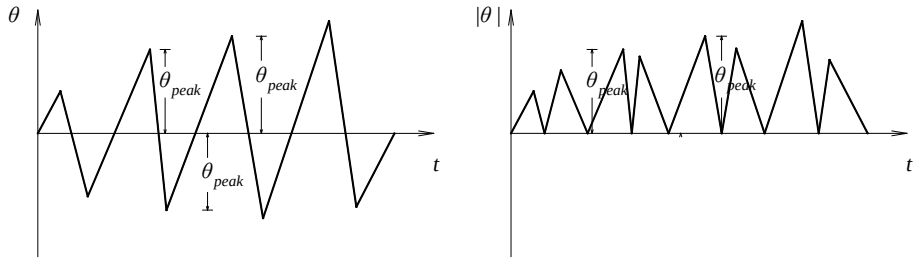

Fig. 13 Amplitudes (θ_{peak}) of interstory drift time history

Fig. 14 is the *CDF* (cumulative distribution function) of θ_{peak} for each intensity (*I*) and each story of FEM model simulation results, where *x* is the drift value. Fig. 15 shows the *CDF* of θ_{peak} for each intensity (*I*) and each story of neural network outputs. According to the FEM simulation model results and neural network outputs, θ_{max} can be selected, and Fig. 16 is a θ_{max} comparison of the FEM results and network outputs. In the *RS-OUT* Coordinate System for each intensity value, data are observed to be distributed aside from a line of which the slope is approximately 1, reflecting that θ_{max} values of FEM results and network outputs of each intensity are highly similar. According to their *CFD*, θ_{mean}, which is the mean value of θ_{peak} for each intensity (*I*), and each story of FEM model simulation results and neural network outputs were calculated. Because the amplitudes of *EQ* for each intensity stage are nearly constant, θ_{peak} in each story of each intensity is nearly constant, and θ_{mean} can be a representative value for all θ_{peak} values in this story of this intensity stage. Fig. b17 is θ_{mean} comparison of FEM results and network outputs. In the *RS-OUT* Coordinate System for each intensity value, data are observed to be distributed aside from a line of which the slope is approximately 1, reflecting that θ_{mean} values of FEM results and network outputs of each intensity are also highly similar.

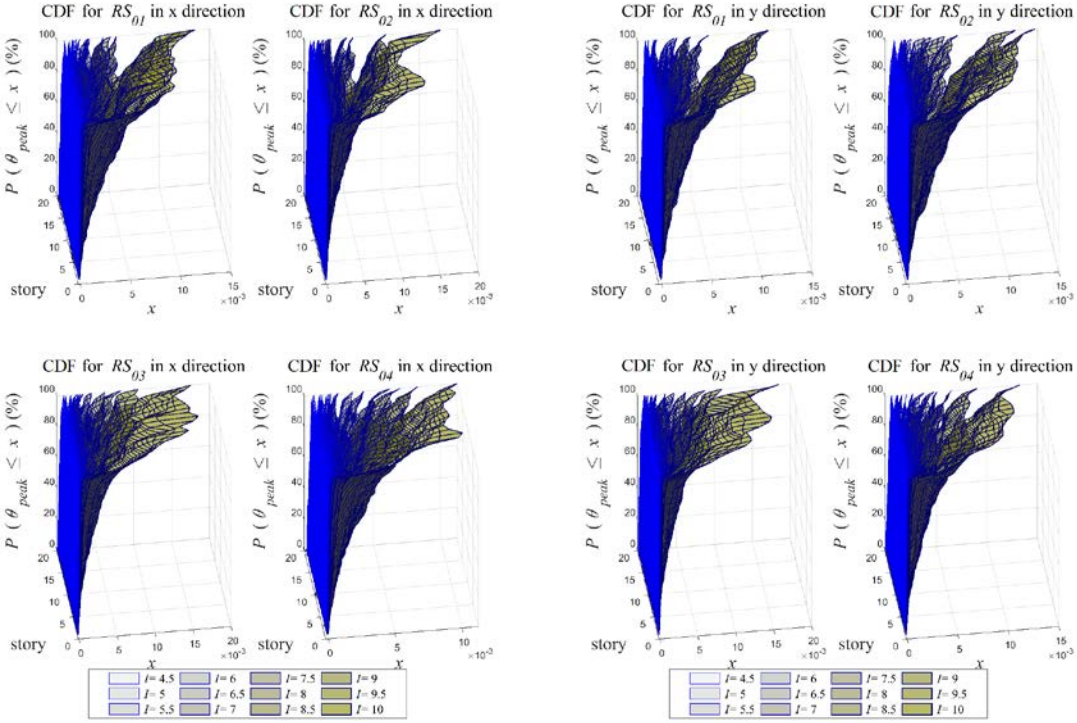
CDF for RS_{01} in x direction
CDF for RS_{02} in x direction
CDF for RS_{01} in y direction
CDF for RS_{02} in y direction
CDF for RS_{03} in x direction
CDF for RS_{04} in x direction
CDF for RS_{03} in y direction
CDF for RS_{04} in y direction
$P(\theta_{peak} \le x)$ (%)
story
x
$\times 10^{-3}$
I= 4.5
I= 5
I= 5.5
I= 6
I= 6.5
I= 7
I= 7.5
I= 8
I= 8.5
I= 9
I= 9.5
I= 10

(a)

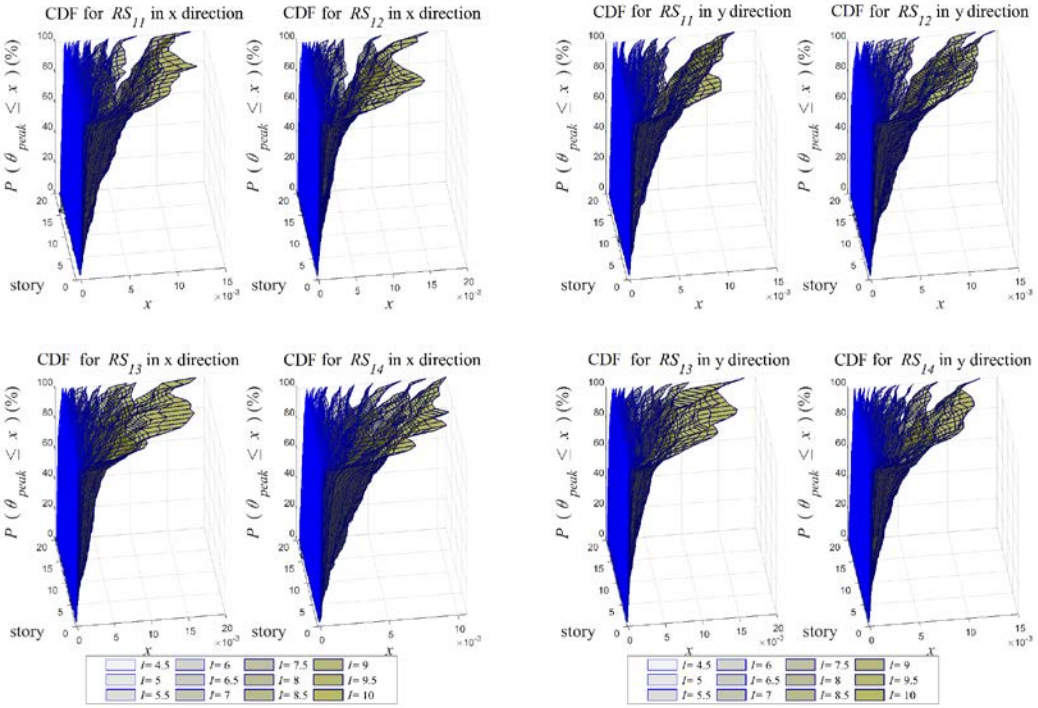
CDF for RS_{11} in x direction
CDF for RS_{12} in x direction
CDF for RS_{11} in y direction
CDF for RS_{12} in y direction
CDF for RS_{13} in x direction
CDF for RS_{14} in x direction
CDF for RS_{13} in y direction
CDF for RS_{14} in y direction
$P(\theta_{peak} \le x)$ (%)
story
x
$\times 10^{-3}$
I= 4.5
I= 5
I= 5.5
I= 6
I= 6.5
I= 7
I= 7.5
I= 8
I= 8.5
I= 9
I= 9.5
I= 10

(b)

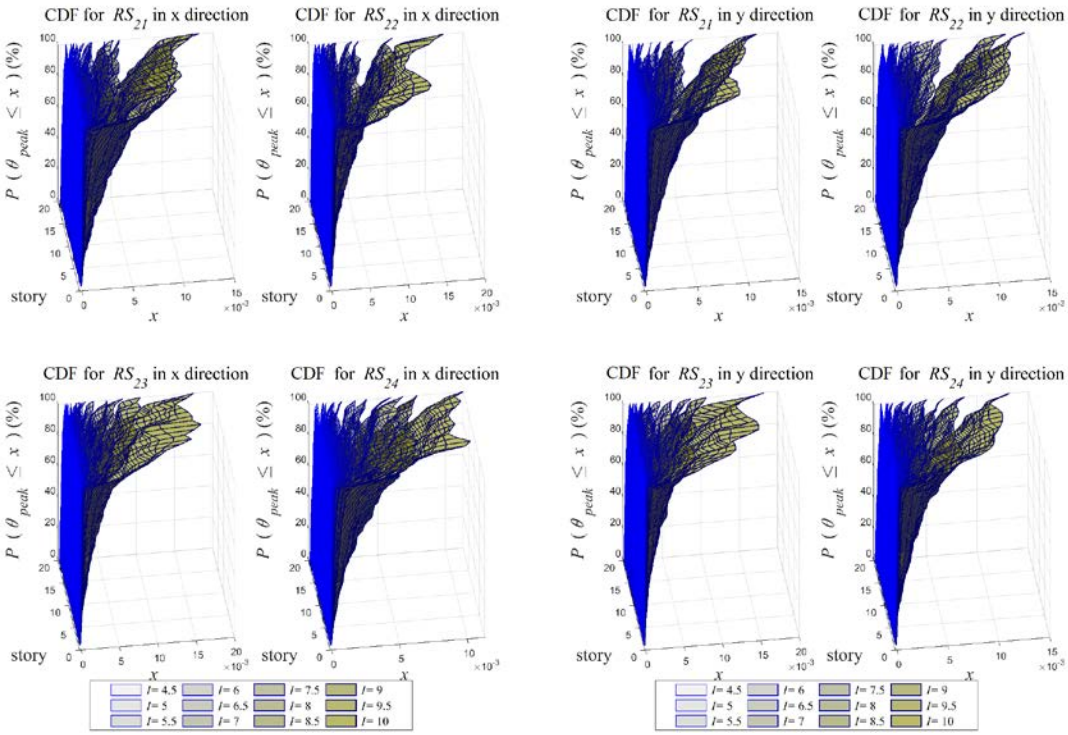

(c)

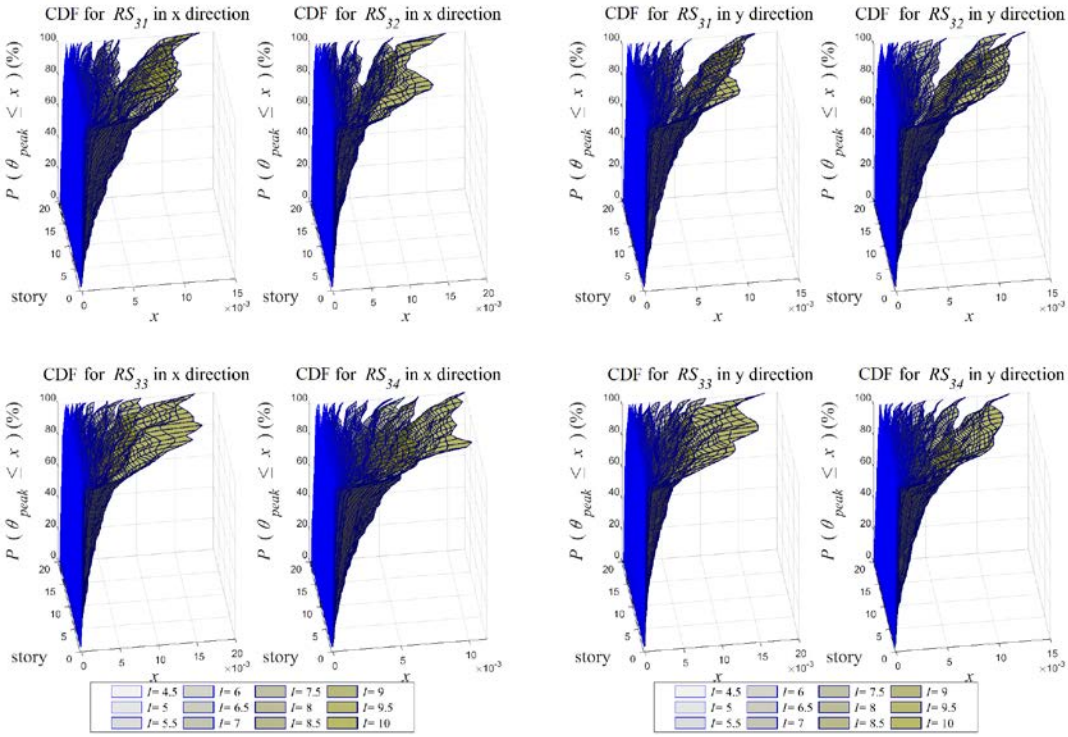

(d)

Fig. 14 *CDF* of θ_{peak} of FEM simulation results: (a) M_0; (b) M_1; (c) M_2; (e) M_3

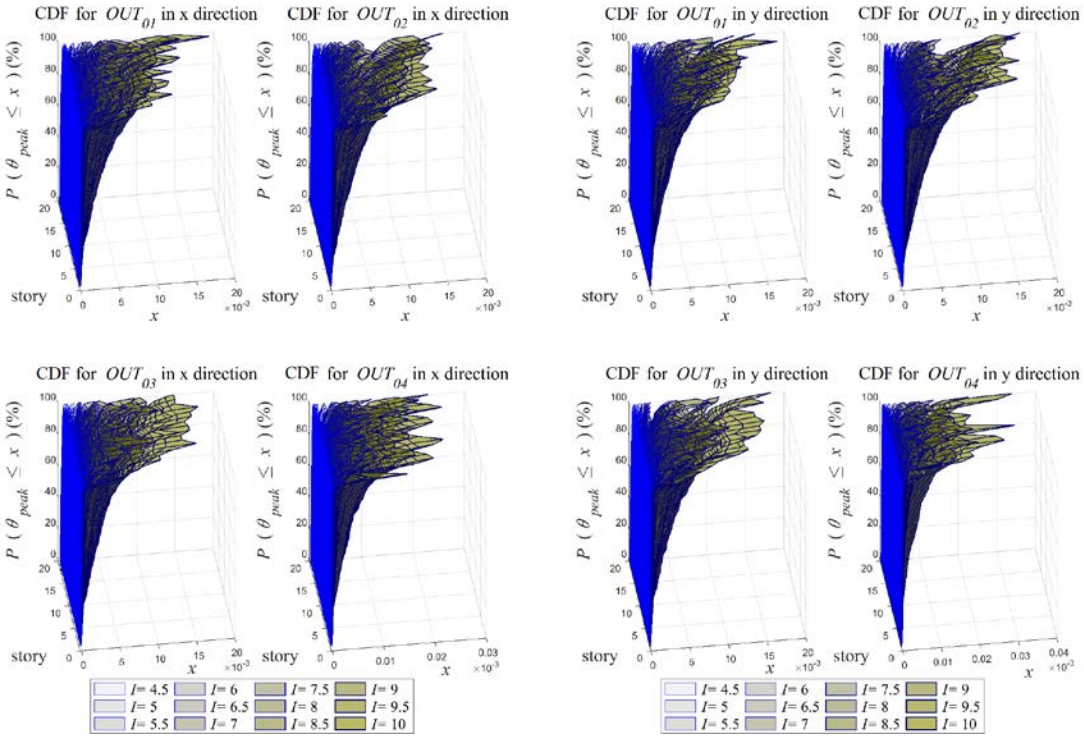
CDF for OUT_{01} in x direction
CDF for OUT_{02} in x direction
CDF for OUT_{01} in y direction
CDF for OUT_{02} in y direction
CDF for OUT_{03} in x direction
CDF for OUT_{04} in x direction
CDF for OUT_{03} in y direction
CDF for OUT_{04} in y direction
$P(\theta_{peak} \mid x)$ (%)
story
x
I= 4.5
I= 5
I= 5.5
I= 6
I= 6.5
I= 7
I= 7.5
I= 8
I= 8.5
I= 9
I= 9.5
I= 10

(a)

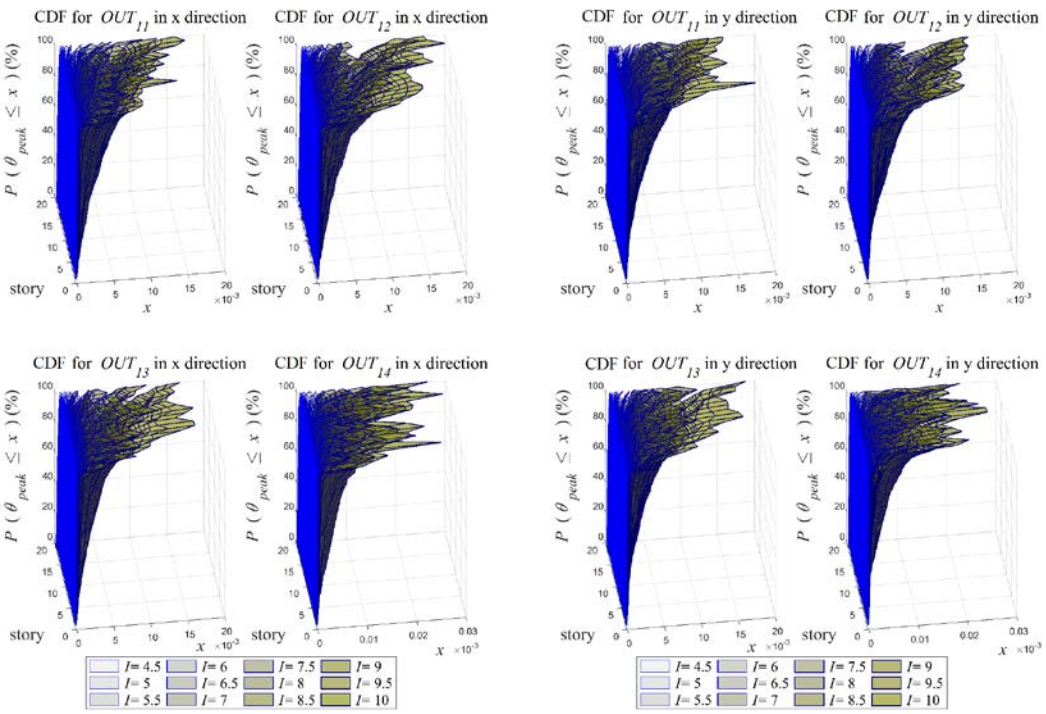
CDF for OUT_{11} in x direction
CDF for OUT_{12} in x direction
CDF for OUT_{11} in y direction
CDF for OUT_{12} in y direction
CDF for OUT_{13} in x direction
CDF for OUT_{14} in x direction
CDF for OUT_{13} in y direction
CDF for OUT_{14} in y direction
$P(\theta_{peak} \mid x)$ (%)
story
x
I= 4.5
I= 5
I= 5.5
I= 6
I= 6.5
I= 7
I= 7.5
I= 8
I= 8.5
I= 9
I= 9.5
I= 10

(b)

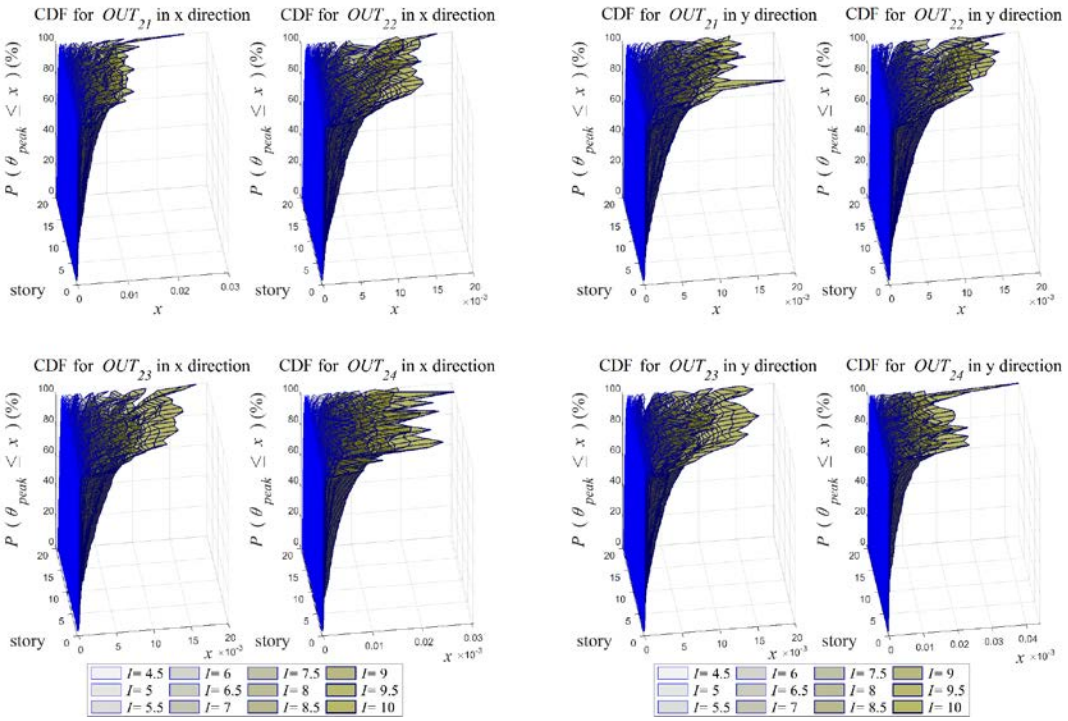

(c)

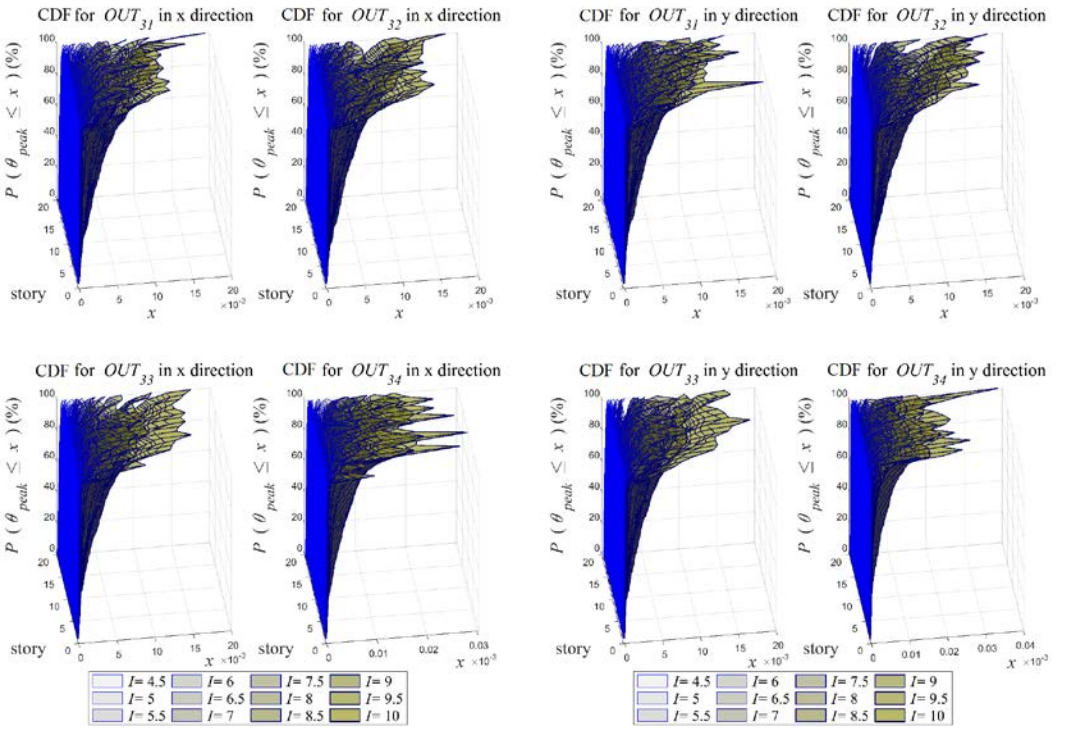

(d)

Fig. 15 *CDF* of θ_{peak} of neural network outputs: (a) M_0; (b) M_1; (c) M_2; (e) M_3

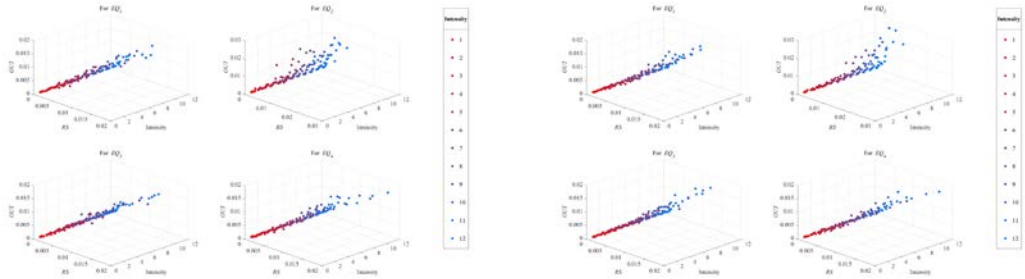

(a)

(b)

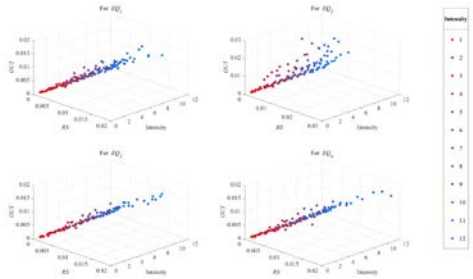

(c)

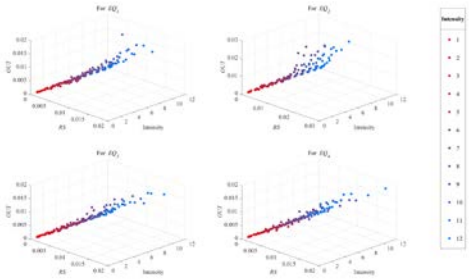

(d)

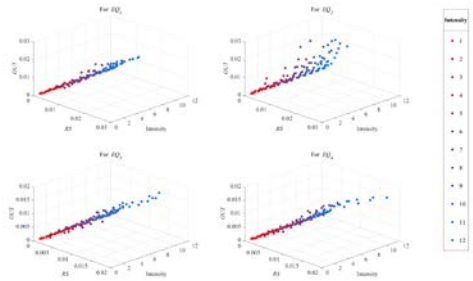

(e)

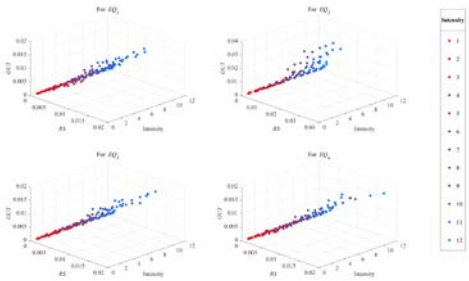

(f)

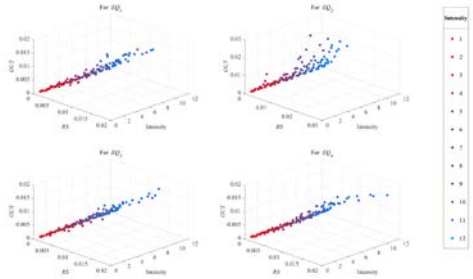

(g)

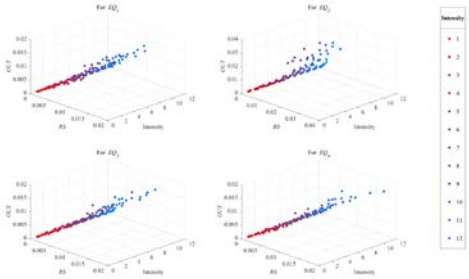

(h)

Fig. 16 θ_{max} comparison of FEM results and network outputs: (a) M_0-x; (b) M_0-y; (c) M_1-x; (d) M_1-y; (e) M_2-x; (f) M_2-y; (g) M_3-x; (h) M_3-y;

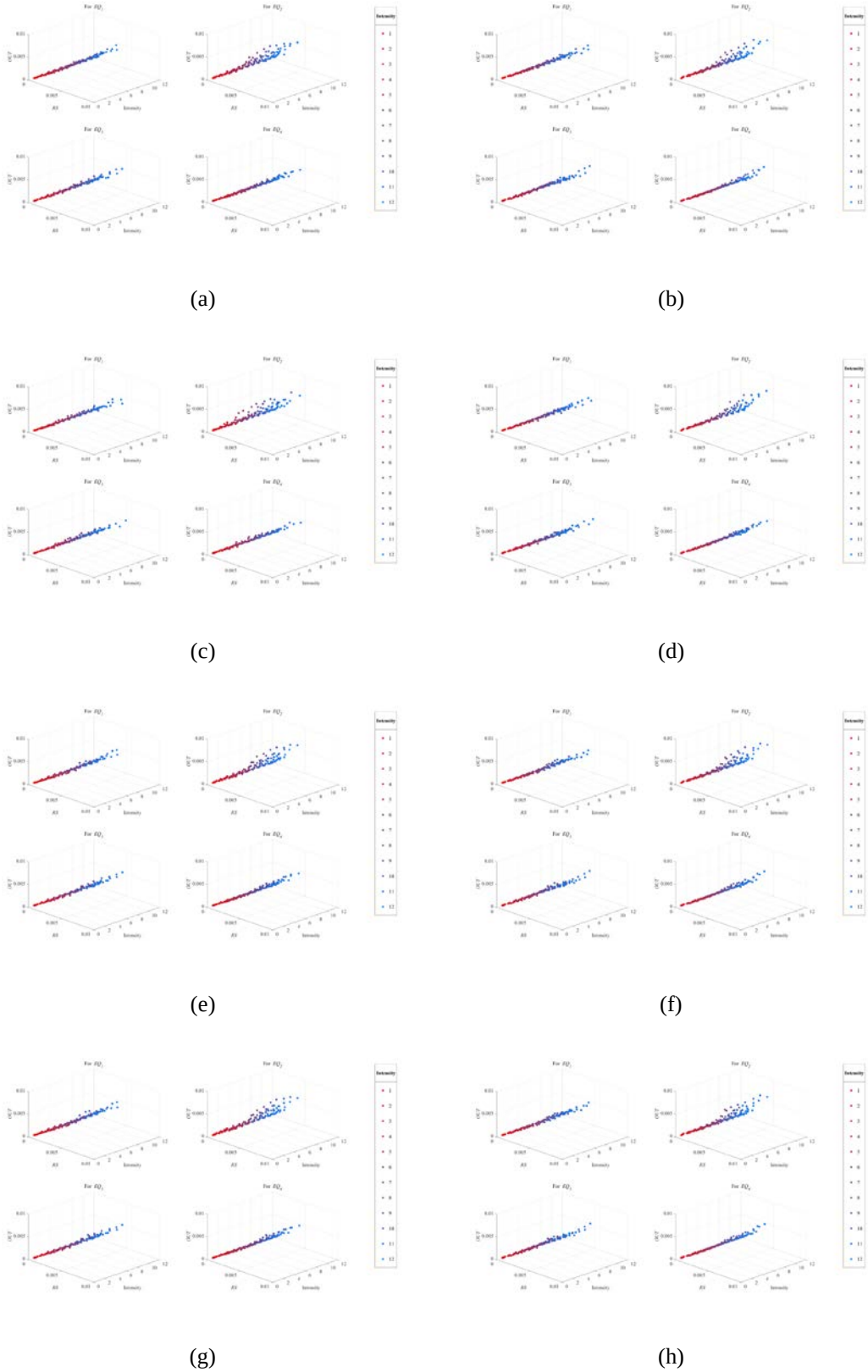

Fig. 17 θ_{mean} comparison of FEM results and network outputs: (a) M_0-x; (b) M_0-y; (c) M_1-x; (d) M_1-y; (e) M_2-x; (f) M_2-y; (g) M_3-x; (h) M_3-y;

The coefficient of determination (r^2) represents quantifying the goodness-of-fit, of which the value is between 0 and 1 and is as large as better fitting (Ritter, A. 2013). It is a statistical measurement to examine the explanation of differences in one variable by the difference in a second variable. For variables x_1, x_2, x_3, …, x_4, their predicted values are $\widehat{x_1}$, $\widehat{x_2}$, $\widehat{x_3}$, …$\widehat{x_n}$, respectively, and r^2 of this fitting is shown as Eq.2.

$$r^2 = \frac{\sum_{i=1}^{n} (\widehat{y_i} - \bar{y})^2}{\sum_{i=1}^{n} (y_i - \bar{y})^2} \quad \textbf{(2)}$$

and $\bar{y}$ is the mean value of variables.

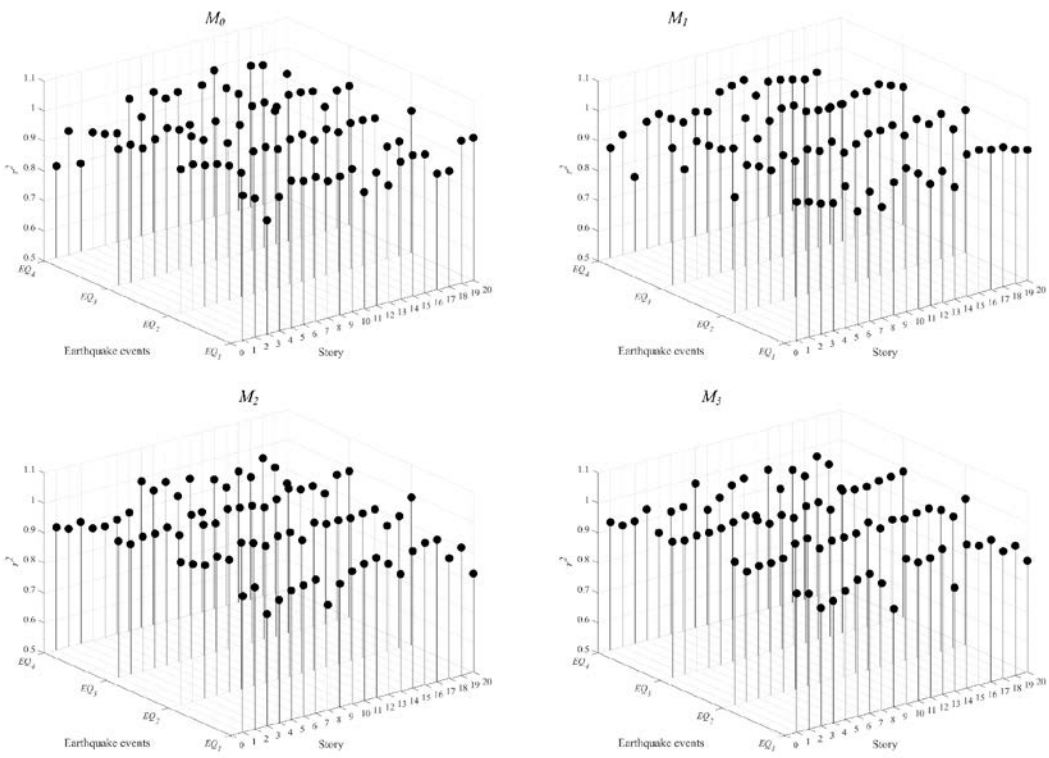

(a)

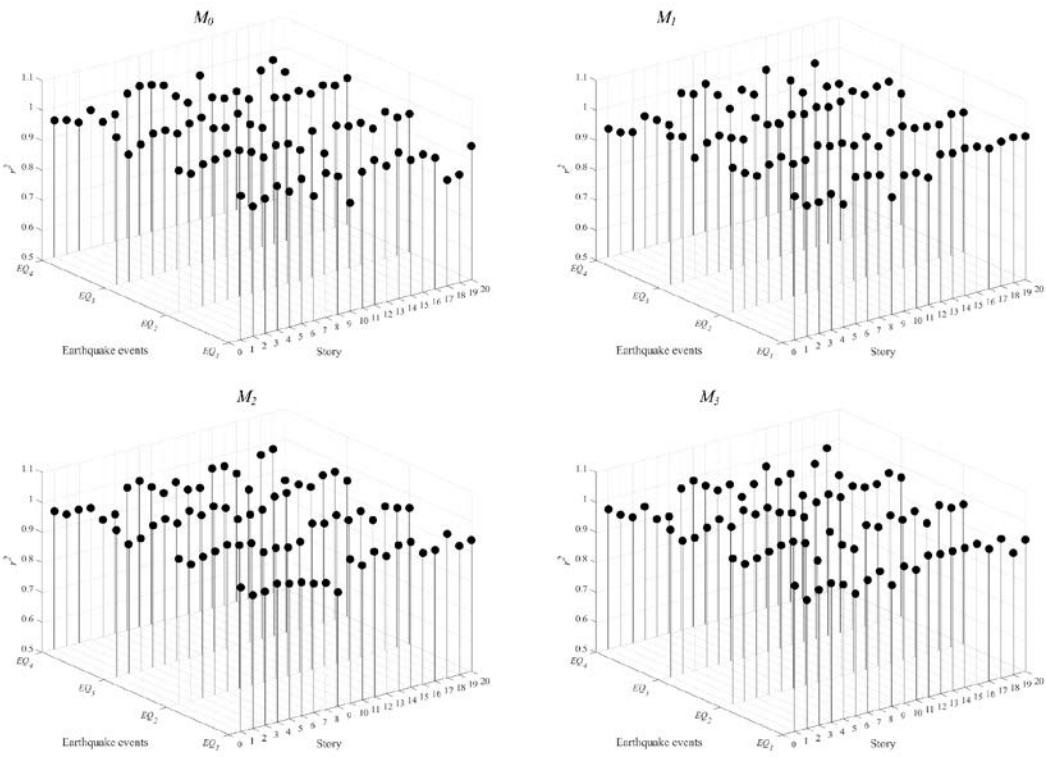

(b)

Fig. 18 r^2 of θ_{max}: (a) x-direction; (b) y-direction

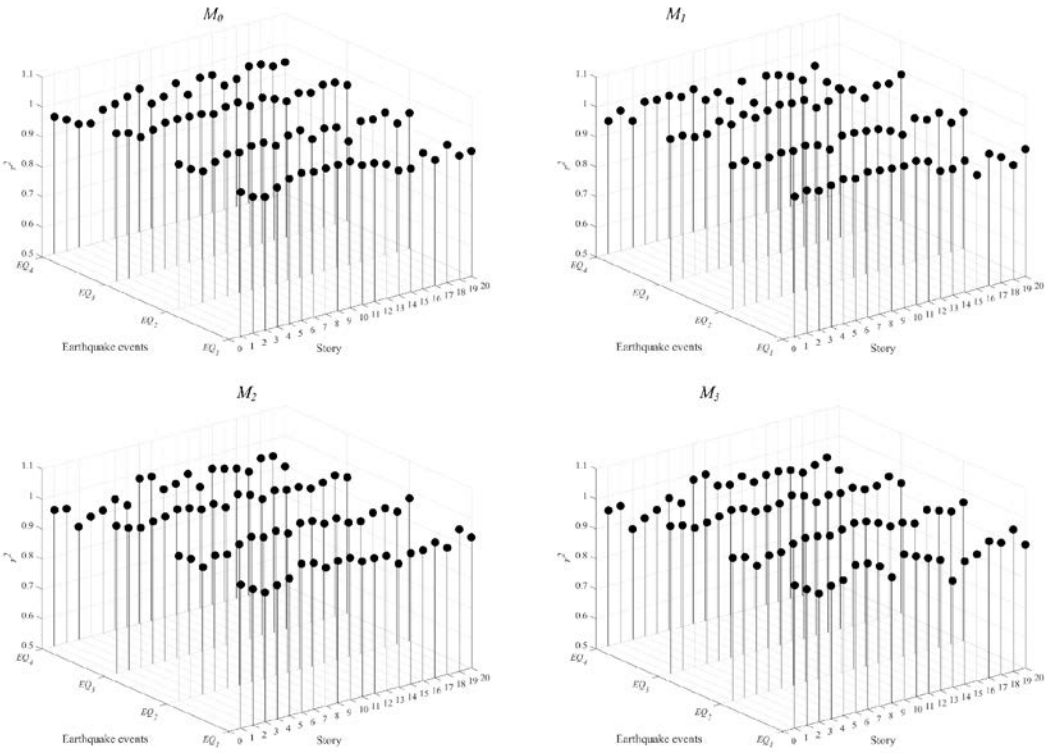

(a)

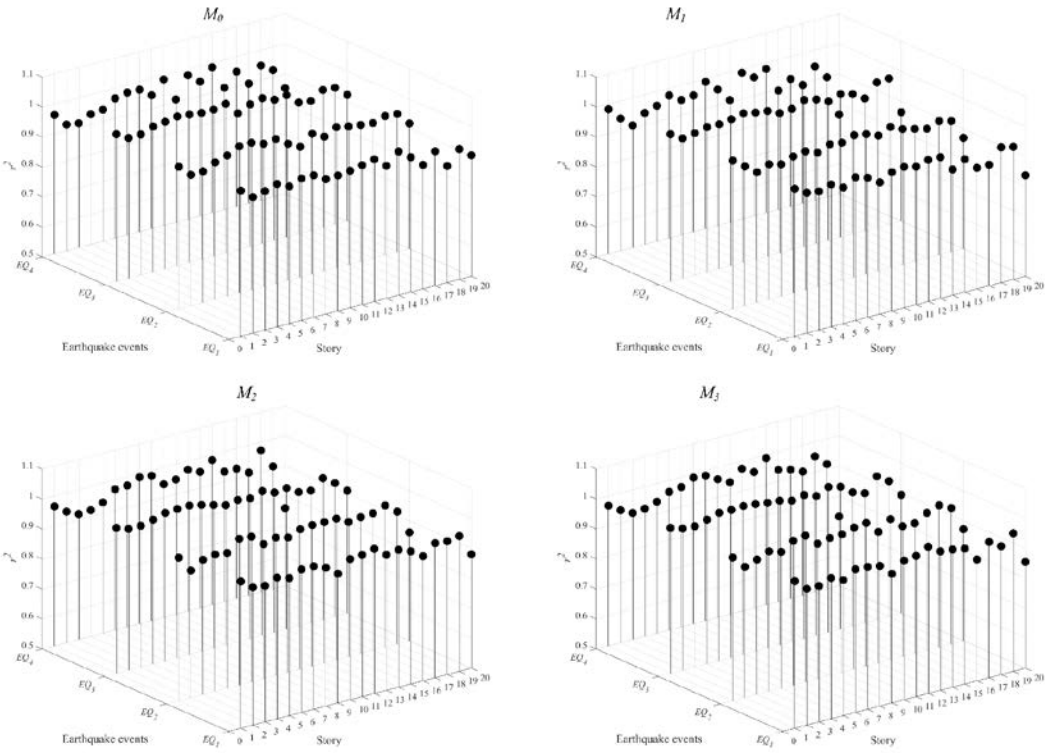

(b)

Fig. 19 r^2 of θ_{mean}: (a) x-direction; (b) y-direction

r^2 values of θ_{max} and θ_{mean} between simulation results of FEM models and neural networks output each story and earthquake events EQ_1, EQ_2, EQ_3, and EQ_4 are used for describing networking fitting accuracy. As shown in Fig. 18 and Fig. 19, the r^2 values of θ_{max} and θ_{mean} are all larger than 0.8, which reflects that more than 80% of the samples, including the training models and testing models of both θ_{max} and θ_{mean}, can be explained by TDNN group fitting. Thus, the Metamodel method, which is based on TDNN groups, can accurately imitate the relationship between earthquake acceleration signals and the seismic response of the frame structure if θ_{max} of each story is selected as the performance objective to measure the failure statuses of frame structures.

4. Conclusions

In this study, a method to build the meta-model for the seismic response of frame structures using TDNN groups was proposed. An accuracy evaluation method that can balance both training time and

accelerable accuracy was proposed. Four frame structure FEM models that are 5×5 spans and 20 stories are applied as examples to show the model establishment and accuracy evaluation process.

Comparing θ_{max} and θ_{mean} of training targets with outputs by TDNN and of testing targets with predicted data by TDNN, in *RS-OUT* Coordinate System for each intensity value, data are distributed aside from a line of which the slope is approximately 1. For these two safety evaluation factors, the FEM results and network outputs of each intensity are highly similar.

The r^2 results reflect that more than 80% of samples, which include training models and testing models of both θ_{max} and $\theta_{mean,}$ can be explained by TDNN group fitting. If θ_{max} of each story is selected as the performance objective to measure the failure status of frame structures, these metamodels are sufficiently accurate.

The average calculation time of these example models is 24 min, and the average time spent by the TDNN models is 0.08 s. The calculation time obviously increased, and it can be applied to Monte Carlo analysis and structural seismic safety early warning.

Acknowledgments

This research was funded by Junior Researcher Grant Yangzhou University (Grant No. 137012122), and this study was financially supported by the China Scholarship Council (CSC) (Grant No. 20180670149). Natural earthquake data were downloaded from PEER Strong Ground Motion Databases (https://peer.berkeley.edu/peer-strong-ground-motion-databases). And the calculation is supported by Institute for Risk and Reliability, University Hannover.

Reference

Chen, Y. , Wang, H. , Xue, A. , Lu, R.(2010). Passivity analysis of stochastic time-delay neural networks. *Nonlinear Dynamics*, 61(1-2): 71-82. DOI:10.1002/stc.226

Chen, Z. , Liu, B. . (2016). Lifelong machine learning. *Synthesis Lectures on Artificial Intelligence & Machine Learning*, 10(3), 1-145. DOI:10.2200/S00737ED1V01Y201610AIM033

EN1998-1.(2004). EC 8: Seismic Design of Buildings. EUROPEAN COMMITTEE FOR STANDARDIZATION.

FEMA P.58.(2012). Seismic Performance Assessment of Buildings. FEDERAL EMERGENCY MANAGEMENT AGENCY, USA.

FEMA356.(2000). PRESTANDARD AND COMMENTARY FOR THE SEISMIC REHABILITATION OF BUILDINGS. FEDERAL EMERGENCY MANAGEMENT AGENCY, USA.

GB50011.(2010). Code for seismic design of buildings. Ministry of housing and urban rural development of the people's Republic of China, China.

Guo, H. , Wang, S. , Fan, J. , Li, S. . (2019). Learning automata based incremental learning method for deep neural networks. *IEEE Access*, 1-1. DOI:10.1109/ACCESS.2019.2907645

Huang, Y. , Han, X., Zhao, L.Y.. (2021). Recurrent neural networks for complicated seismic dynamic response prediction of a slope system. Engineering Geology, 289:106198. https://doi.org/10.1016/j.enggeo.2021.106198

Kikkawa, H. , Shoji, F. , Tanaka, J. , Kataoka, F. , Satou, H..(1993) . Negative-type photosensitive polyimide precursors developable with aqueous alkaline solutions. *Polymers for Advanced Technologies*, 4(4): 268-276. DOI:10.1002/pat.1993.220040407

Li, Z., Hoiem, D.(2017). Learning without forgetting. *IEEE transactions on pattern analysis and machine intelligence*, 40(12): 2935-2947. DOI:10.1007/978-3-319-46493-0_37

Mander, J. B., Priestley, M. J. N., and Park, R. (1988). Theoretical stress-strain model for confined concrete. *Journal of Structural Engineering*, 114(8): 1804-1826, https://doi.org/10.1061/(ASCE)0733-9445(1988)114:8(1804)

Mathworks. (2021). Neural Network Training Concepts. Matlab R2021 Help Center. https://www.mathworks.com/help/deeplearning/ug/neural-network-training-concepts.html

Mayhan, J., Simmons, A., Cummings, W.(1981). Wide-band adaptive antenna nulling using tapped delay lines. *IEEE Transactions on Antennas and Propagation*, 29(6): 923-936. DOI:10.1109/TAP.1981.1142694

Menegotto, M. and Pinto, P. E. (1973). Method of analysis for cyclically loaded R.C. plane frames including changes in geometry and non-elastic behavior of elements under combined normal force and bending. Proc., IABSE Symposium on Resistance and Ultimate Deformability of Structures Acted on by Well Defined Repeated Loads, IABSE, Zurich, Switzerland, 15-22.

Molina, D. , et al. (2011). Comparison of TDNN and RNN performances for neuro-identification on small to medium-sized power systems. Computational Intelligence Applications In Smart Grid (CIASG), 2011 IEEE Symposium on IEEE. https://doi.org/10.1109/CIASG.2011.5953344

Park, Y. , Ang, Alfredo H.-S. (1985). Mechanistic seismic damage model for reinforced concrete. *Journal of Structural Engineering*, 111(4), 722-739. DOI:10.1061/(ASCE)0733-9445(1985)111:4(722)

Pomerleau, D..(1991). Efficient training of artificial neural networks for autonomous navigation. *Neural computation*, 3(1): 88-97. DOI:10.1162/neco.1991.3.1.88

Powell, G. H. , Chen, P. F. . (1986). 3d beam-column element with generalized plastic hinges. *Journal of Engineering Mechanics*, 112(7), 627-641. https://doi.org/10.1061/(ASCE)0733-9399(1986)112:7(627)

Rahman, M.M., Nahar, T.T., Kim, D..(2021). FeView: Finite element model (FEM) visualization and post-processing tool for OpenSees. *SoftwareX*, 15: 100751. https://doi.org/10.1016/j.softx.2021.100751

Ritter, A., Muñoz-Carpena, R.(2013). Performance evaluation of hydrological models: Statistical significance for reducing subjectivity in goodness-of-fit assessments. *Journal of Hydrology*, 480: 33-45. DOI:10.1016/j.jhydrol.2012.12.004

Sherstinsky, A. (2020). Fundamentals of Recurrent Neural Network (RNN) and Long Short-Term Memory (LSTM) Network. *Physica D: Nonlinear Phenomena*, 404. https://doi.org/10.1016/j.physd.2019.132306

Shoaib, M. , Shamseldin, A. Y. , Khan, S. , Sultan, M. , Ali, I. . (2019). Input selection of wavelet-coupled neural network models for rainfall-runoff modelling. *Water Resources Management*, 33(2). DOI:10.1007/s11269-018-2151-x

Waibel, A., Hanazawa, T., Hinton, G., Shikano, K., Lang, K. J.(1989). Phoneme Recognition Using Time-Delay Neural Networks, IEEE Transactions on Acoustics, Speech, and Signal Processing, 37(3): 328-339.

Wei, Z. , Li, C. , Peng, G. , Chen, Y. , & Zhang, Z. . (2017). A deep convolutional neural network with new training methods for bearing fault diagnosis under noisy environment and different working load. *Mechanical Systems & Signal Processing*, 100(FEB.1), 439-453. DOI:10.1016/j.ymssp.2017.06.022

White, H.. (2014). Learning in artificial neural networks: a statistical perspective. *Neural Computation*, 1(4): 425-464. DOI:10.1162/neco.1989.1.4.425

Zhang, H. (2021). Method to Generate Artificial Earthquake Accelerations with Time Domain Enhancement and Attenuation Characteristics. *Ain Shams Engineering Journal*. (Under review)

Zhang, H., Cao, P., Z., Wu, K., Ren, L., J. (2019-a).Two-Step Seismic Calculating Method and Seismic Features of SRC-RC Hybrid Frame Structure. *Journal of Performance of Constructed Facilities*, 5(33). https://doi.org/10.1061/(ASCE)CF.1943-5509.0001317

Zhang, H., Ca O, P. , Wu, K. , Xu, C. , Ren, L. . (2019-b). Lateral bearing capacity and stiffness calculation method of SRC-RC columns. *KSCE Journal of Civil Engineering*.06. https://doi.org/10.1007/s12205-019-0232-x

Zhang, R. , Chen, Z. , Chen, S. , Zheng, J. , Buyukozturk, O. , Sun, H..(2019). Deep long short-term memory networks for nonlinear structural seismic response prediction. *Computers & Structures*, 220:55-68. https://doi.org/10.1016/j.compstruc.2019.05.006

Zhou, J. , Li, E. , Yang, S. , Wang, M. , Mitri, H.. (2019). Slope stability prediction for circular mode failure using gradient boosting machine approach based on an updated database of case histories. *Safety Science*, 118:505-518. https://doi.org/10.1016/j.ssci.2019.05.046